DETECTION AND CLASSIFICATION OF DIABETIC FOOT THERMOGRAMS USING DEEP LEARNING

A DISSERTATION

SUBMITTED IN PARTIAL FULFILLMENT OF THE REQUIREMENTS FOR THE AWARD OF THE DEGREE
OF

MASTER OF TECHNOLOGY

IN

SIGNAL PROCESSING AND DIGITAL DESIGN

Submitted by

Aarushi Jain

(2K20/SPD/01)

Under the supervision of

PROF. S. INDU

DEPARTMENT OF ELECTRONICS AND COMMUNICATION

DELHI TECHNOLOGICAL UNIVERSITY

(Formerly Delhi College of Engineering)

Bawana Road, Delhi -110042

MAY, 2022

DEPARTMENT OF ELECTRONICS AND COMMUNICATION ENGINEERING
DELHI TECHNOLOGICAL UNIVERSITY
(Formerly Delhi College of Engineering)
Bawana Road, Delhi-110042

CANDIDATE'S DECLARATION

I, **Aarushi Jain,** student of M.Tech (Signal Processing and Digital Design), hereby declare that the project Dissertation titled **"Detection and Classification of Diabetic Foot Thermograms Using Deep Learning"** which is submitted by me to the Department of Electronics and Communication Engineering, Delhi Technological University, Delhi in partial fulfilment of the requirement for the award of the degree of Master of Technology is original and not copied from any source without proper citation. This work has not previously formed the basis for the award of any Degree, Diploma Associateship, Fellowship, or other similar title or recognition.

Place: Delhi **Aarushi Jain**

Date: 30th May 2022

DEPARTMENT OF ELECTRONICS AND COMMUNICATION ENGINEERING
DELHI TECHNOLOGICAL UNIVERSITY
(Formerly Delhi College of Engineering)
Bawana Road, Delhi-110042

CERTIFICATE

I hereby certify that the Project Report titled "**Detection and Classification of Diabetic Foot Thermograms Using Deep Learning**" which is submitted by **Aarushi Jain**, **2K20/SPD/01** of Electronics and Communication Department, Delhi Technological University, Delhi, in partial fulfilment of the requirement for the award of the degree of Master of Technology, is a record of the project work carried out by the students under my supervision. To the best of my knowledge, this work has not been submitted in part or full for any Degree or Diploma to this University or elsewhere.

Place: Delhi — Prof. S. Indu

Date: 30th May 2022 — **SUPERVISOR**

ACKNOWLEDGEMENT

I would like to express my heartfelt gratitude to Prof. S. Indu for her constant support and valuable guidance throughout the duration of this project. Also, I would like to thank her for giving me this opportunity to explore and gain treasured knowledge about the areas of the domain of this noble project. Without her constant supervision, this project would not have been possible. New ideas and direction from her made it probable for me to sail through various areas of this project which were new to me.

I would also express my gratefulness to Dr. N. S. Raghava, HOD, Department of Electronics and Communication Engineering, who encouraged me in many ways for the smooth completion of my research work. Special acknowledgments to all the faculty members of the ECE Department and other supporting staff for their guidance during my M. Tech course.

Aarushi Jain

ABSTRACT

Diabetes is a long-lasting disorder which is also a cause for high mortality rate. Diabetic Foot Ulcers (DFU) is a condition associated with diabetes. Diabetes, a chronic ailment generating high blood sugar is a key reason for mortality and lifestyle degradation. Thermography is an emerging and non-invasive medical imaging practice that can be used for body disorder diagnosis. Temperature difference from the usual body temperature is the basis of this technique. In the recent scenario, Deep Learning (DL) algorithms serve as a smart and precise approach for classifying DFUs with the utilization of thermograms.

In this work, performance of transfer learning based DL networks (AlexNet and Resnet-101) has been analyzed in classifying foot thermograms into CG (Control Group) and DM (Diabetic Mellitus) groups. Furthermore, a novel and enhanced technique (ProNet), is proposed in this paper. It is designed by combining the best features of both AlexNet and ResNet. By simulation results obtained in this work, it can be inferred that AlexNet has greater accuracy (96.8%) than that obtained in the existing work. In addition to this, ResNet101 yields better results than AlexNet (accuracy of 97.9%). ProNet, the proposed methodology achieves improved performance in terms of accuracy (as high as 98.9%) and other metrics like precision, specificity and F1 Score.

Also, this work evaluates the performance of transfer learning DL networks (DarkNet-19 and DarkNet-53) in multiclass classification of DFUs based on Thermal Change Indices (TCIs). Moreover, an improved and novel methodology (Pro-Multi-Net), is proposed. The optimum features of both DarkNet-19 and DarkNet-53 are combined to design this algorithm. As per simulation results, it can be deduced that all the three methods implemented have higher accuracy than the techniques applied in the existing work. Furthermore, DarkNet-53 yields better results than DarkNet-19 (overall accuracy of 92.8%). Pro-Multi-Net, the proposed network achieves an improved overall accuracy of 95.5%. Also, precision, recall and F1-Score values are also obtained for all the classes.

- Chapter-1 gives an introduction to diabetic foot ulcers, infrared thermography and anomaly detection procedure in diabetic foot. Moreover, it provides a brief outline of DFU classification using multiple DL techniques.

- Chapter-2 discusses the literature review of work done in this domain along with a glimpse of proposed work is discussed in this chapter.

- Chapter-3 explains the techniques implemented in this work for binary classification and multiclass classification of diabetic foot thermograms including the novel and proposed methodology.

- Chapter-4 includes the results and discussion. It provides the simulation details and explains the results obtained in this work. Also, a comparative analysis of all the methods implemented is given.

- Chapter-5 explains the conclusion and future work that can be carried out in this domain.

CONTENTS

LIST OF FIGURES

LIST OF TABLES

LIST OF ABBREVIATIONS

1. DFU	−	Diabetic Foot Ulcer
2. IR	−	Infrared
3. MIT	−	Medical Infrared Thermography
4. TTM	−	Thermal Texture Mapping
5. ROI	−	Region Of Interest
6. MTD	−	Mean Temperature Difference
7. GLCM	−	Gray Level Co-occurrence Matrix
8. CAD	−	Computer Aided Diagnosis
9. NC	−	Neuro-Computing
10. FL	−	Fuzzy Logic
11. EC	−	Evolutionary Computing
12. ML	−	Machine Learning
13. DL	−	Deep Learning
14. CG	−	Control Group
15. DM	−	Diabetic Mellitus
16. ICA	−	Independent Component Analysis
17. DWT	−	Discrete Wavelet Transform
18. HOS	−	Higher Order Spectra
19. HPF	−	High Pass Filter
20. LPF	−	Low Pass Filter
21. LBP	−	Local Binary Pattern
22. LTE	−	Laws Texture Energy
23. PPV	−	Positive Predictive Value
24. SVM	−	Support Vector Machine
25. CNN	−	Convolutional Neural Network
26. TCI	−	Temperature Change Index
27. RFN	−	Rate of False Negatives
28. RFP	−	Rate of False Positives
29. SD	−	Standard Deviation
30. STD	−	Standard Temperature Difference
31. FLC	−	Fully Connected
32. CL	−	Convolutional Layer
33. MATLAB	−	MATrix LABoratory
34. SGDM	−	Stochastic Gradient Descent with Momentum
35. FN	−	False Negative
36. FP	−	False Positive

CHAPTER - 1

INTRODUCTION

This chapter gives an introduction to diabetic foot ulcers and importance of infrared thermography in the diagnosis of the same. It also explains the anomaly detection procedure in diabetic foot. Moreover, it provides a brief outline of diabetic foot ulcer categorization using multiple deep learning practices.

1.1 Introduction

The leading global causes for deprivation in lifestyle standards and death cases include Diabetes. Several difficulties associated with this disorder (vision loss, kidney failure and heart attacks) have a considerable effect on health as well as ergonomics [1-3]. Diabetic foot is a key consequence of diabetes in which the ulceration risk is amplified by plantar region pressure and sensitivity loss. Diabetic Foot Ulcer (DFU) is a result of such condition.

Health conditions have been indicated by temperature since earlier times. Skin surface temperature and its distribution is regarded as a valuable indicator of an abnormality in human body. In thermography, infrared camera is used to detect blood flow and heat patterns in tissues of the body [4]. But thermography subsequently stopped being used in medical practices. This was due to untutored technicians which highly vague information. With the advancement of quantum well IR photodetector camera having high precision, progressive algorithms of image processing, qualified technicians, there is a revival of interest in thermography in medical treatments [5].

1.2 Medical Infrared Thermography

Medical infrared thermography (MIT) is an ancient technology in which variation in body heat indicates causal medical condition. A graphical depiction of heat is known as IR thermography. The image produced by it with the usage of photographic film that is sensitive to IR radiation is a thermograph. Contact, computer assisted and

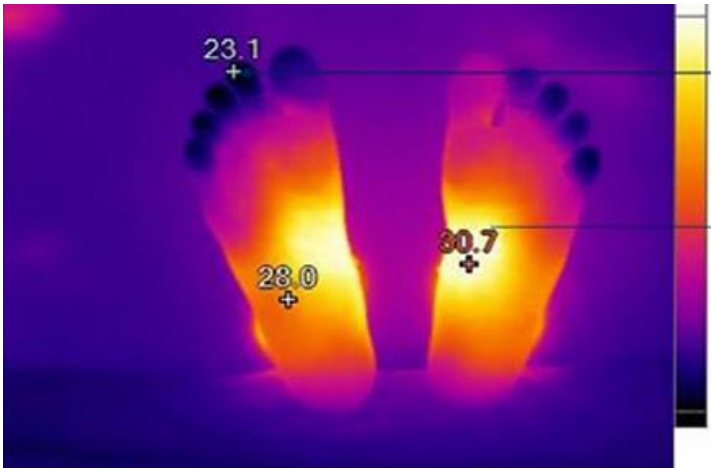

Fig 1.1 Foot Thermogram [5]

remote sensing thermography are various types [6-8]. Static, dynamic (active and subtraction, DAT,) Thermal Texture Mapping (TTM), multimodality, multispectral and sensor fusion are different categories of IR based imaging methodologies.

1.2.1 Advantages of MIT

IR energy radiated from skin surface is captured by IR thermal image. Several medical imaging technologies image human body's anatomy and structure. But unlike these, thermography has the capability of imaging skin's thermovascular appearance [9]. Some of the benefits of MIT are:

1. As a diagnosis tool, temperature has hopeful results in detecting numerous diseases such as rheumatoid arthritis, breast cancer, Raynaud's syndrome and osteoarthritis early.

2. Poor radiance does not have any contrary effect on the image as thermal imaging has less sensitivity towards light.

3. It is noncontact, non-invasive, and non-radiant. Therefore, the imaging equipment doesn't subject any hurtful radiation on patients.

4. An object's surface temperature distribution can be effortlessly obtained by a thermal imager.

5. Computer aided diagnostic system is practicable and accurate because of growth in software image processing proficiencies and thermal sensing apparatus.

IR thermography is contactless and henceforth has the benefit over other evaluation tools like vibration sensation and monofilament tests. It confines the needless pressure and contact that might disturb temperature reading and lessen the infection spreading through gear [10]. Furthermore, it allows measurement of whole foot temperature distribution irrespective of surfaces or shapes [11]. Thus, analyzing the temperature distribution of plantar can be operative for early discovery of DFUs.

1.3 Abnormality Detection Process in Diabetic Foot

Detection of abnormalities in diabetic foot follows the procedure as shown in Fig 1.2. The steps involved are:

1) **Image acquisition:** IR thermogram acquisition must be done in controlled temperature. Diverse imaging setups for thermal IR image procurement of foot influence on the accuracy of detection and classification of DFUs. Thermal imaging camera is used for this purpose.

2) **Segmentation:** Right and left foot are segmented from each other. Also, segmentation of feet from the background is done. Morphological process is used to remove segmented region if it spreads outside the foot edges. Many methods are used for segmentation such as Canny, Otsu, Sobel algorithms. Also, snake's model can be used.

3) **Partitioning:** It involves extraction of Region of Interest (ROI) from the segmented foot to execute analysis. ROIs are the areas which have high risk of ulceration.

4) **Feature Extraction:** It consists of extracting statistical features like correlation and Mean Temperature Difference (MTD) between corresponding pixels in left and right foot. Also, contrast, homogeneity, Gray Level Co-occurrence Matrix (GLCM), energy can be extracted.

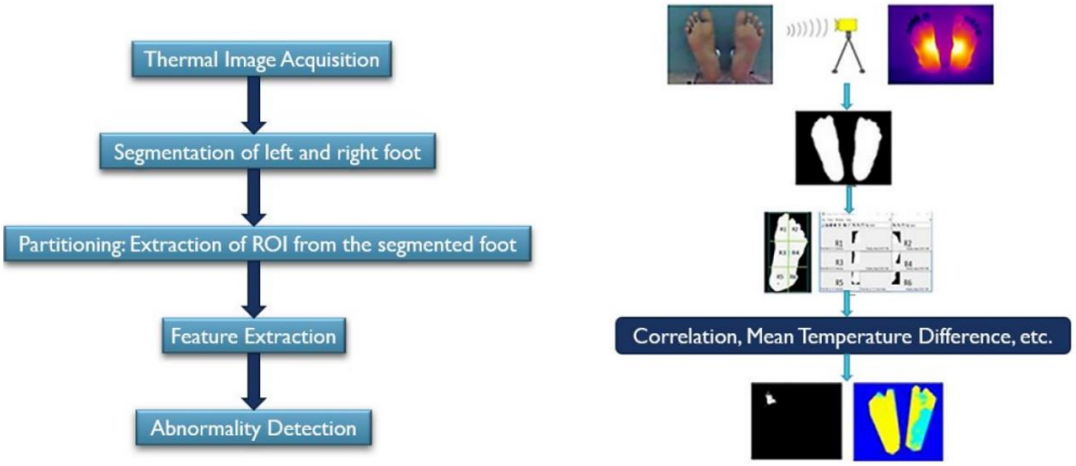

Fig 1.2 Abnormality Detection in Diabetic Foot

5) **Abnormality Detection:** Any abnormality in human physiology can be detected early from a thermal IR image with precise temperature measurement. Presence of ulcer in diabetic patients is characterized by a hot region.

1.4 Diabetic Foot Classification

Neuropathic, ischemic and neuro-ischemic are various classes of DFUs. Usually, neuropathic ulcers happen at 40% rate but the ischemic ulcer rate is lone 10% [12]. In diabetic patients, hotness can be a pre-ulceration symptom of neuropathic foot. Whereas, ischemic foot is characterized by an absence of adequate arterial blood flow from heart to the foot. This disease and symptom is accompanied with a cold temperature of skin. Hence, coldness can be a pre-ulceration sign of ischemic foot. Arteriopathy and neuropathy situations describe the ischemic and neuropathic foot respectively. Patients in whom both ailments occur together are neuro-ischemic.

There has been shift in conventional manual analysis of data to CAD (Computer-Aided Diagnosis) for purpose of detection [13]. Contemporary intelligent diagnosis for MIT image analysis combines several soft practices of soft computation such as NC (Neuro-Computing), FL (Fuzzy Logic), EC (Evolutionary Computing) and ML (Machine Learning) for classification of low, high, moderate, normal or diseased. Deep learning (DL) models are a means for further precise intelligent systems [14].

Control Group (CG) comprises of persons which are susceptible to a lesser ulceration of foot in contrast to Diabetic Mellitus (DM) group (has higher probability of DFU) [15]. Fig 1.3 (a) and (b) represent the CG and DM group thermograms respectively. The mean difference of angiosomes of a DM group person and reference values given by angiosomes of CG is indicated by TCI (Thermal Change Index) value [16]. TCI values can be utilized for classification of DFUs into multiple levels as depicted in Fig 1.4.

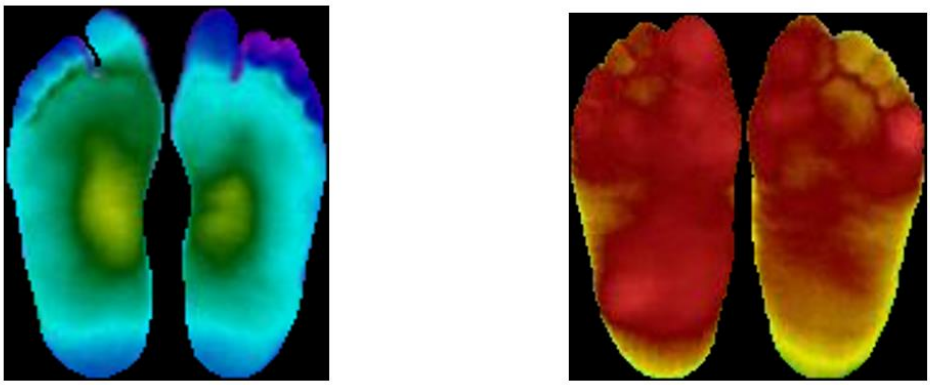

Fig 1.3 Foot Thermograms: (a) CG (Control Group); (b) DM (Diabetic Mellitus) [15]

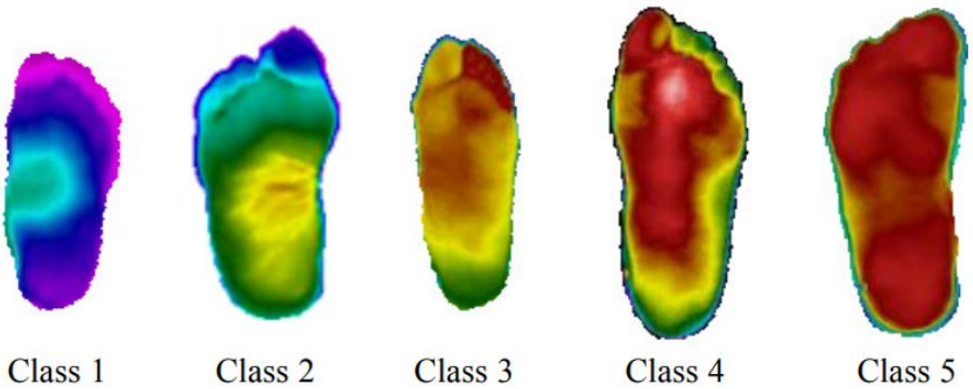

Fig 1.4 Five Classification Levels of Diabetic Foot Thermogram [16]

CHAPTER - 2

LITERATURE REVIEW

In numerous diabetic foot studies, IR thermography has been used which associate plantar temperature discrepancies with DFU complications . An introduction to work done in this domain along with a glimpse of proposed work is discussed in this chapter.

2.1 Introduction

Bagavathiappan et al. considered the association between foot temperature and diabetic neuropathic patients in 2010 [17]. It was observed that non-neuropathy patients recorded lesser foot temperature between 27°C and 30°C unlike in the case of diabetic patients (32°C to 35°C).

Bharara et al. [18] and Nagase et al. [10] provided a classification method for plantar thermographic patterns on the basis of concept of angiosomes. Differences in control group because of reduced participants might be the disadvantage. Age and gender are unparalleled in control group, leading to confusing data analysis factors.

Agurto et al. [12] projected a technique to categorize diabetic patients (neuropathic) in 2015 using ICA process and IR thermography. Some preliminary frames are not involved in analysis. Few areas (especially toes), need stabilization to evade important movements.

A descriptive review on various practices used in diabetic foot complications on the basis of stress test, asymmetry and temperature distribution examination is provided by Hernandez-Contreras [19].

Further in this chapter, review of five current research papers published in this domain will be provided.

2.2 Segmentation and Feature Extraction Algorithms

This section provides a review of segmentation and feature extraction algorithms implemented in previous research work including the detailed procedure, results and merits and demerits of each technique.

2.2.1 Segmentation: Snake's Algorithm

Maximum of the conventional practices compared both feet separately or did the analysis of whole image. But, geometric deformation frequently makes such an assessment stimulating and sometimes inaccurate. Separating each foot into numerous regions and after that comparison of both feet can enhance efficiency of segmentation. It was found that regions with peak temperatures had the highest DFU risk in each foot [20].

1) Procedure:

- **Thermal Image Acquisition:** 59 thermographic images of plantar foot (as depicted in Fig 2.1) of diabetic patients are used, captured by FLIR A320 (thermal camera with high resolution [21-23]) that is used to extract foot surface isotherms.

- **Segmentation:** To separate two feet from background, snakes (active contour model) is used. Also, right foot is separated from left. This model is a system for delineation of object from a practicably noisy image. It consists of a repeatedly controlled spline under the influence of external constraint and image forces. Snake's energy function is represented by (2.1) and (2.2).

  Snake's Energy Function:

$$E_{snake}^{total} = \int_0^1 E_{snake}(s(k))\, dk \tag{2.1}$$

$$= \int_0^1 (E_{int}(s(k)) + E_{image}(s(k)) + E_{con}(s(k)))\, dk \tag{2.2}$$

- **Partitioning:** Interpolation methodology is used that divides plantar into diverse parts [24].

- **Clustering:** Fuzzy c means is an algorithm used for clustering in this paper. This clustering algorithm is used for recognizing the highest temperature plantar regions [25].

2) Results:

Segmentation model (snake's) was applied two times for every image. First time for the separation of right foot from the left. Second time-left foot from the background (Fig 2.2 and Fig 2.2.). Each foot was segregated into three parts - Part 1 - big toe, Part 2 - ball of foot, Part 3 – heel as depicted in Fig 2.3. Partitioning is done to identify the areas which are at higher ulceration risk. Fuzzy c means was executed for three cases. Primary and secondary hottest regions were discovered for each foot. Primary hottest region is utmost likely for being a doubtful region for future DFU [20].

Fig 2.1 Thermographic Image of a Subject [20]

Fig 2.2 Separated (a) Right and (b) Left Foot from Background [20]

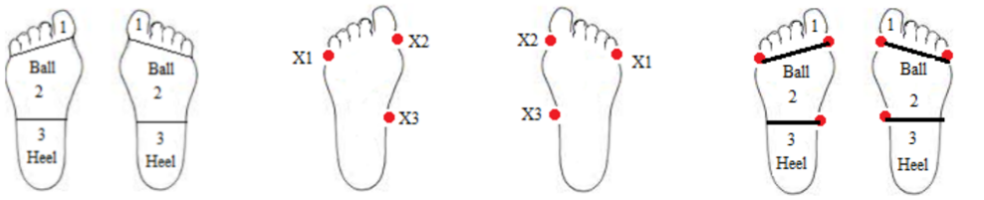

(a) Three different parts of the plantar

(b) Locations of x1, x2, and x3

(c) Two interpolated lines and three parts

Fig 2.3 Partitioning of Two Plantar Feet 20]

(a) Whole image (b) Zone 1 (c) Zone 2 (d) Zone 3

Fig 2.4 Separated parts of the Left Foot [20]

(a) Whole Image (b) Zone 1 (c) Zone 2 (d) Zone 3

Fig 2.5 Separated Parts of the Right Foot [20]

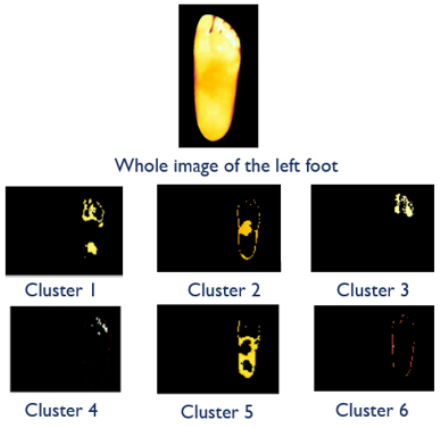

Fig 2.6 Clustering of the Left Foot [20]

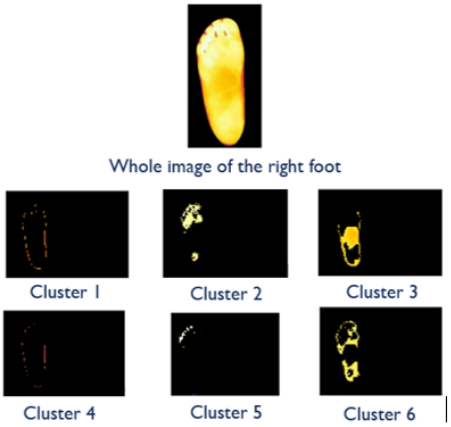

Fig 2.7 Clustering of the Left Foot [20]

3) Advantages:

The merits of algorithms used in the paper are listed in Table 2.1.

Table 2.1 Advantages of Proposed Methods

ALGORITHM	ADVANTAGES
Snakes algorithm Segmentation	• Snakes can be controlled by involving the input of a user • Provides a robust solution • Insensitive to noise • Snakes are easy to operate
Interpolation Partitioning	• Permits more specific results than comparing the mean temperatures of two entire feet
Fuzzy c means Clustering	• Provides more accurate results due to the fuzzy nature of infrared images

2.2.2 Feature Extraction: DWT and HOS

Plantar temperature distribution gives particulars associated with blood perfusion damage. Blood circulation is drastically condensed with the variation in temperature pattern. The purpose of this paper was developing an early detection scheme for DFU with the usage of plantar foot thermograms [15]. Patterns of plantar thermographic images amongst diabetes and normal cases are classified. This can be used as a diagnosis instrument in clinics for medical support in identifying the extent of DFU.

1) Procedure:

- **Thermal Image Acquisition:** Foot thermographic images of 33 healthy people were obtained from SGH. Also 33 images were procured of persons with type 2 diabetes from DMC. VarioCAM was the thermal imaging camera used.

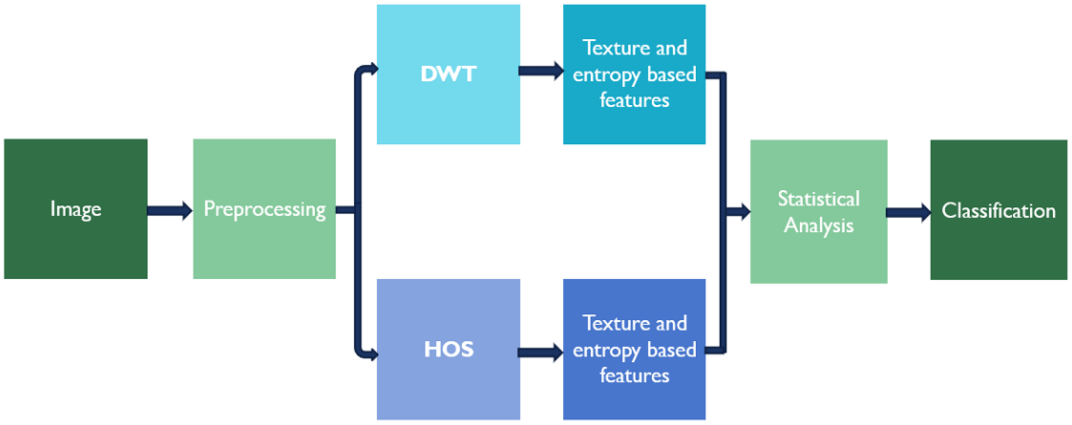

Fig 2.8 Flow Diagram of the Proposed Methodology [15]

- **Segmentation:** Polygon with 16 points was used for delineation of plantar region of foot. Warping procedure transformed segmented region into standard size and shape [26]. DWT and HOS methods are used. Radon transform is used to convert images into 1D data before HOS [27]. DWT alters a 2D signal by exposing over down sampling of HPF and LPF. 2-level DWT is performed with db8 mother wavelet [28,29].

- **Feature extraction:** Entropy and texture features are obtained from decomposed images. Methodologies used are - GLCM), Hu's invariant moment, LBP, LTE and entropies [30-34]. Features are graded by p-values (student t-test). Classification algorithm used is SVM. The flowchart of the proposed methodology is represented by Fig 2.8.

2) Results:

Only 27 clinically substantial features with p-value less than 0.0001 are chosen. The cH2_LME22 has lowermost (0.00002) and 2_HOS36 has peak (0.00014) p-values [15]. These features recorded greater mean for normal than diabetic group.

SVM classifier yielded good results with the use of only five features. Maximum classification accuracy - 89.39%, sensitivity - 81.81%, PPV - 96.43% and specificity - 96.97% were found [15]. The results are represented by Fig 2.9 – 2.11.

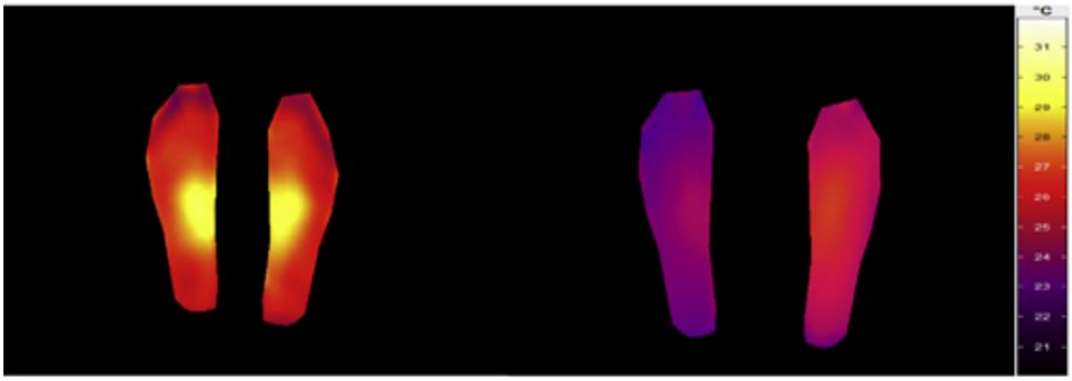

(a) Normal (b) Diabetes without neuropathy

Fig. 2.9 (a) - (b) Segmented Feet Thermograms [15]

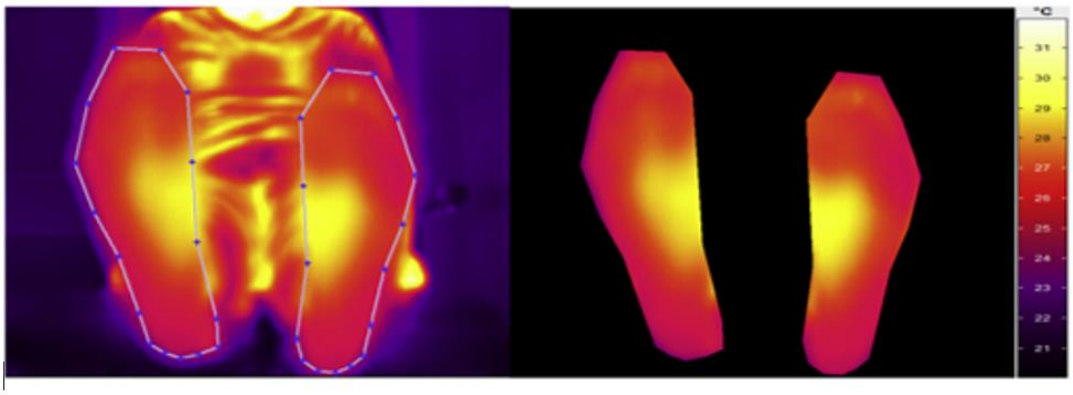

(a) Delineation using polygon (b) Region of Interest

Fig. 2.10 (a)-(b) Segmentation of Plantar Foot [15]

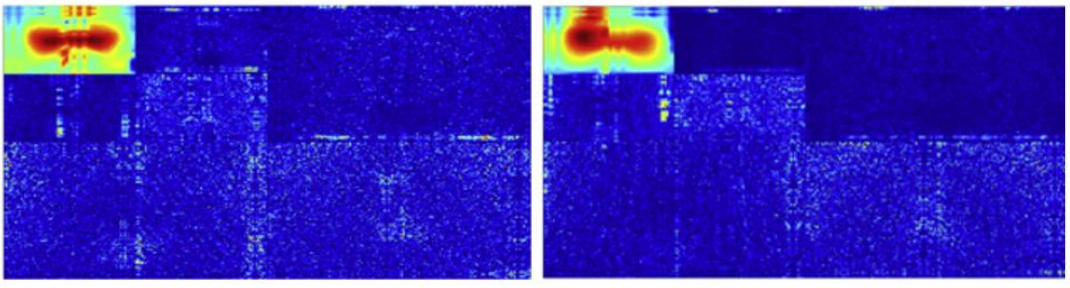

(a) Diabetic foot thermogram (b) Normal foot thermogram

Fig. 2.11 (a) - (b) Two-level DWT [15]

3) Merits and Demerits:

Merits and demerits of the proposed methods are listed in Table 2.2 as shown.

Table 2.2 Merits and Demerits of the Proposed Algorithm

MERITS	DEMERITS
• DWT and HOS coefficients can capture the minute sudden changes in the pixels efficiently • Method is simple, easy, and accurate. • Fast - used only five features to achieve the highest performance • Reliable - same number of subjects with matching age groups and gender are taken • Obtained clear thermal patterns for the two classes	• Used only 66 subjects (33 normal and 33 diabetes). • Semi-automated system • IR thermography is expensive.

2.3 Review of Classification Methodologies

This section gives a detailed literature survey of the classification techniques used.

2.3.1 MobileNet

In MIT, deep learning is used for DFU evaluation. Aim of this work includes studying temperature distribution in plantar foot surface. It was done for normal and diabetic subjects to assess the capability of MIT for early diagnosis of type 1 and type 2 DFUs. Automated testing system for DFU is proposed [35]. Existing clinical processes are correlated with MIT to examine precision of system. The process, results and merits and demerits of the research are described as follows:

1) Procedure:

- **Thermal Image Acquisition:** 62 diabetic patients -38 male and 24 female (with DM) are taken. Also 20 nondiabetic cases (average age - 42 years, SD - 12 years) are imaged at KIER, Bangalore.

- **Segmentation:** It is done using a mask secured in position for both feet by snake's method [36]. Performance is examined using Jaccard index, RFP and RFN as represented by (2.3) – (2.5).

$$Jaccard\ Index = \frac{(GT \cap SI)}{(GT \cup SI)} \tag{2.3}$$

$$RFN = \frac{FN}{FN+TP} \tag{2.4}$$

$$RFP = \frac{FP}{FP+TN} \tag{2.5}$$

- **Region of Interest (ROI):** 6 ROI are detected: hallux (bigger toe), plantar arch other toes region, lateral foot (middle) and heel (outer and inner regions) [37].

- **Feature extraction:** MTD and correlation for four healthy and 4 diabetic subjects is computed.

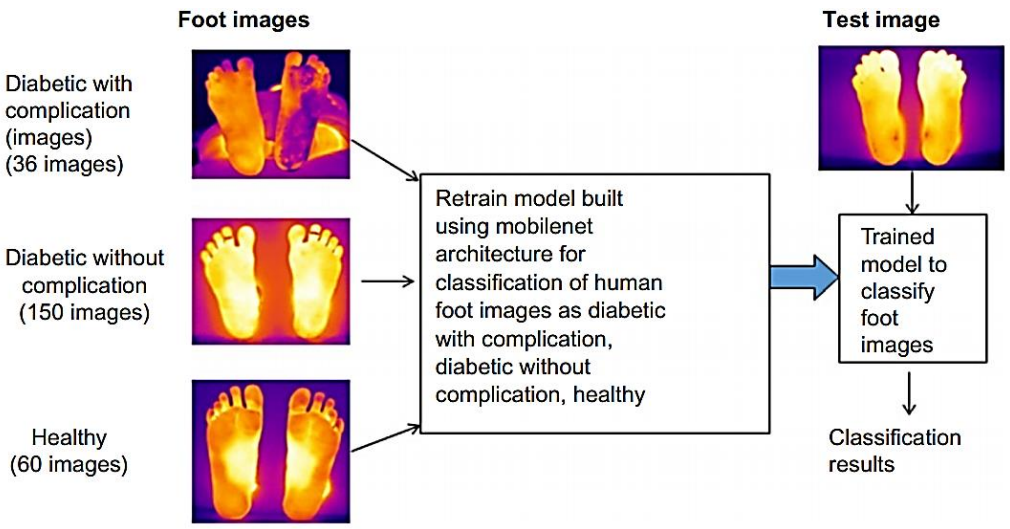

Fig 2.12 Classification System [35]

- **Classification:** Transfer learning is used. It consisted of pretrained DL CNN model known as MobileNet. Classification of DFU was done into healthy and diabetic without and with complications. The classification methodology is shown in Fig 2.12.

2) Results:

STD has symmetrical nature across all conforming regions in healthy subjects (both feet). At plantar arch region, temperature is extremely high because of butterfly pattern. Also, it is minimum 1.5°C greater than other regions. Patients with DFU had temperature variance of 2.2°C [35].

Correlation coefficients found between both feet are higher than 0.7 in the case of healthy subjects. It was from 0.4 to 0.7 in maximum diabetic patients. Right foot had greater temperature than left in regions 3, 2, and 1 in all cases. Average accuracy found was 93.61% for each class [35]. The results of segmentation is shown in Fig 2.13. Fig 2.14 depicts the patterns in healthy and diabetic subjects.

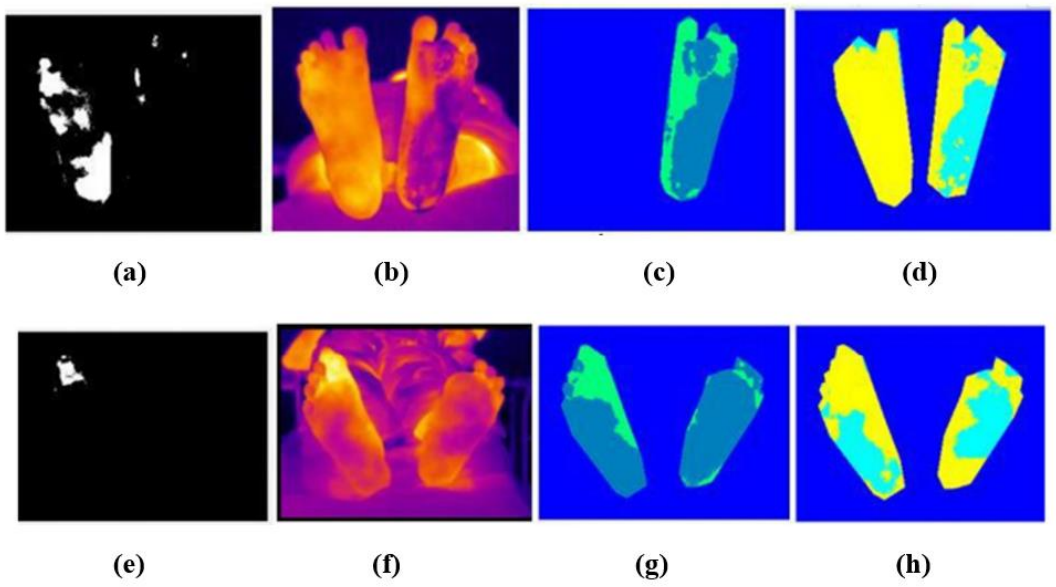

Fig. 2.13 (a, e) Segmented hot regions, (b, f) IR thermal image of diabetic patient, (c, g) segmented cold regions by inbuilt multilevel thresholding, and (d, h) segmented cold region using proposed thresholding method [35]

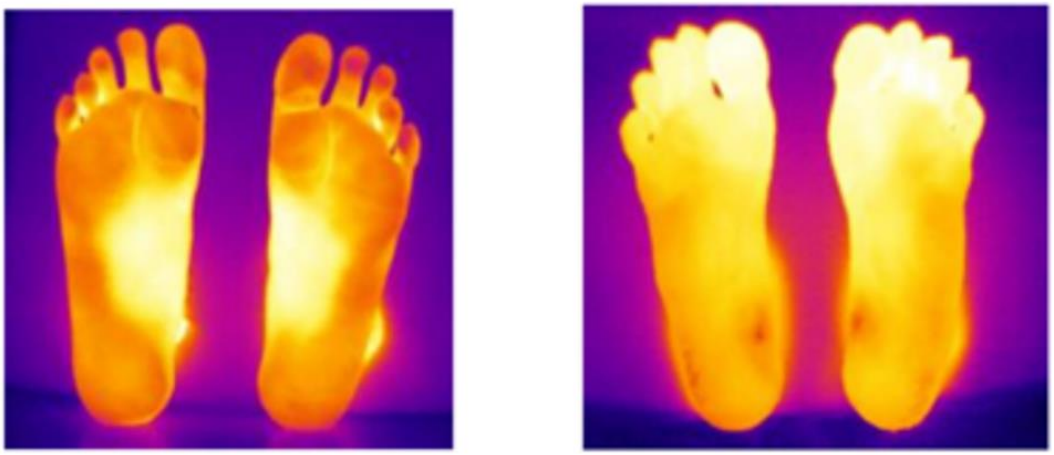

(a) (b)

Fig. 2.14 (a) Butterfly Pattern: Healthy Subject; (b) Hyperthermia in Diabetic Subject

3) Merits and Demerits:

Table 2.3 lists the advantages and disadvantages of the techniques implemented in the research.

Table 2.3 Merits and Demerits of the Proposed Techniques

MERITS	DEMERITS
• Left and right mask for segmentation: to automate the process for all images contained in a folder - saves lot of time and energy • Pretrained model - can be retrained for our own problem in few hours. • Model is able to distinguish between different categories with greater confidence.	• Dataset – small - has to be built with more images • Need to have more control over the parameters - to fine tune the classification and to quantify the level of complication as different categories.

2.3.2 Support Vector Machine

Symmetric temperature and texture distributions are a characteristic of CG thermogram. Asymmetry is found in DM groups. In literature, asymmetric analysis in temperature is one of the common analyses for identifying DFU. Aim was to design an efficient algorithm detection of DFU with asymmetry analysis of IR thermal images [38].

1) Procedure:

- **Thermal Image Acquisition:** 24 - CG and 36 – DM (Total image inputs: 60). These included participants from 30 - 65 years (male and female). Thermal imaging camera - FLIR E60 was used.

- **Segmentation:** Algorithm used - region growing [39]. DF coloured images are transformed into grayscale images. Segmentation of right and left regions of DF is performed from colour image inputs. Also, they are detached from background.

- **ROI:** 5 foot bone heads behindhand the phalanxes of calcaneal heel and toe tops: index, great, middle, little, fourth toe [40,41].

- **Feature extraction:** To extract 2^{nd} order texture characteristics from ROIs, GLCM was used [42-44]. For all the ROIs, SD of temperature and mean is obtained and they are recorded as feature vectors.

- **Asymmetry analysis:** For obtaining extracted temperature and texture feature difference between the two foot regions (contralateral and ipsilateral), this pointer is utilized. For a sole image, ROIs found: 11 (660 for 60 input images) [38].

- **Classification:** SVM algorithm is implemented. Fig 2.15 depicts the flow diagram of the method used. Training thermograms: 140 (70 each for DM and CG); Testing: 520 are used.

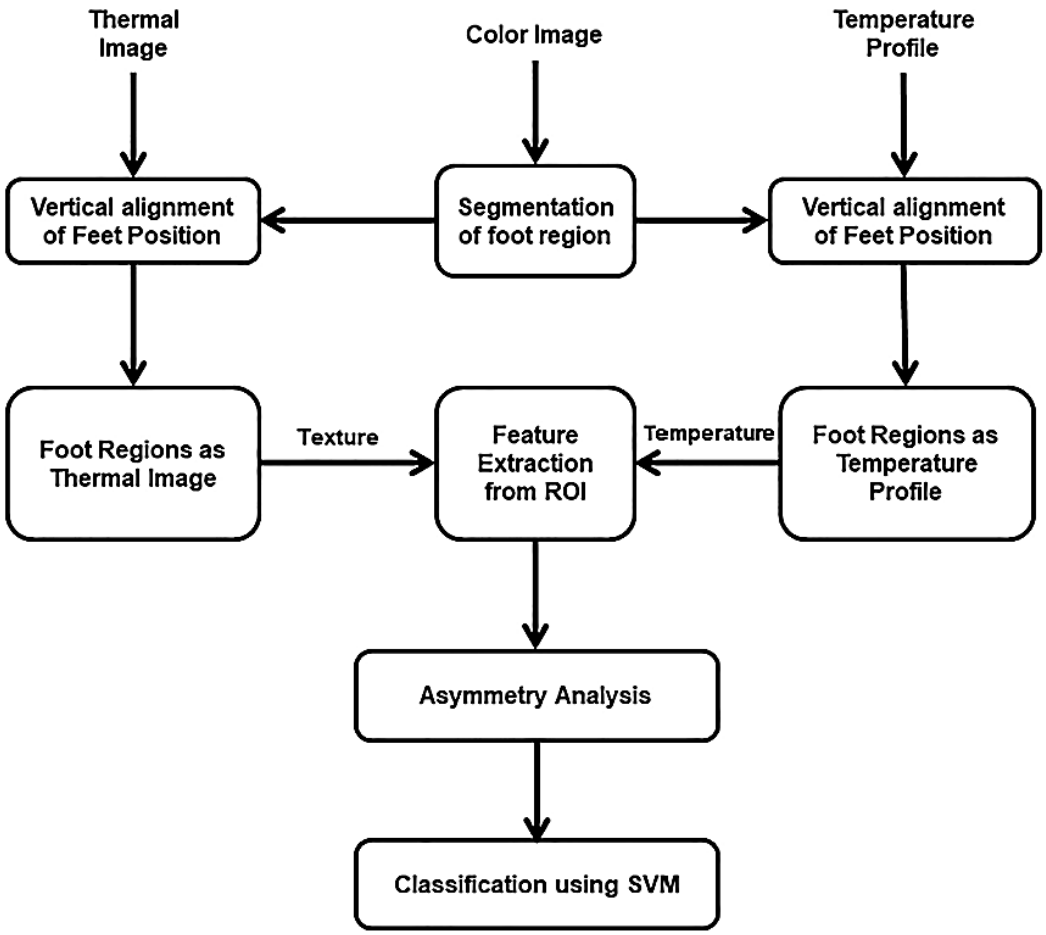

Fig. 2.15 Flowchart of the Proposed Method [17]

2) Results:

Asymmetry in texture features for CG was small and for DM group it was large. Mean SD of extracted features was obtained. 12 GLCM and 2 temperature features were obtained. The features were categorized into ulcer and normal using SVM. Accuracy - 91.23%, specificity - 91.50% and sensitivity - 92.41% were calculated [38].

The results of methodology proposed in this work are shown in Fig 2.16 - 2.18. The DF thermograms for CG and DM groups are depicted in Fig 2.16. Segmentation results for both groups (left; right foot) are shown by Fig 2.17. ROI or principal regions at risk for growing complications in DF are depicted by Fig 2.18.

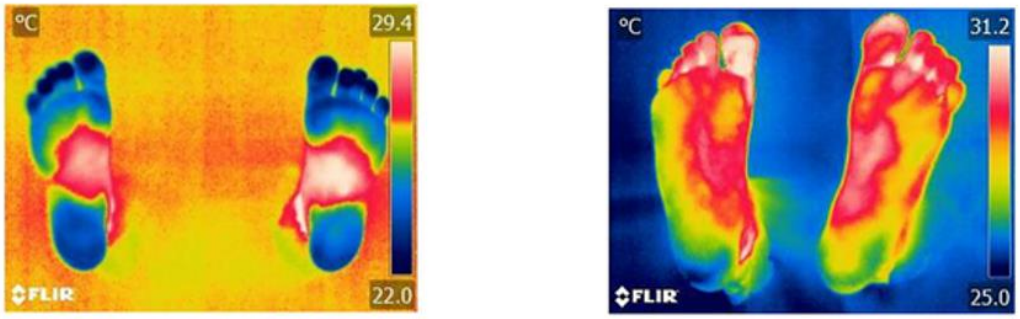

(a) (b)

Fig. 2.16 Thermal Image of the Foot - (a) Control, (b) DM group [38]

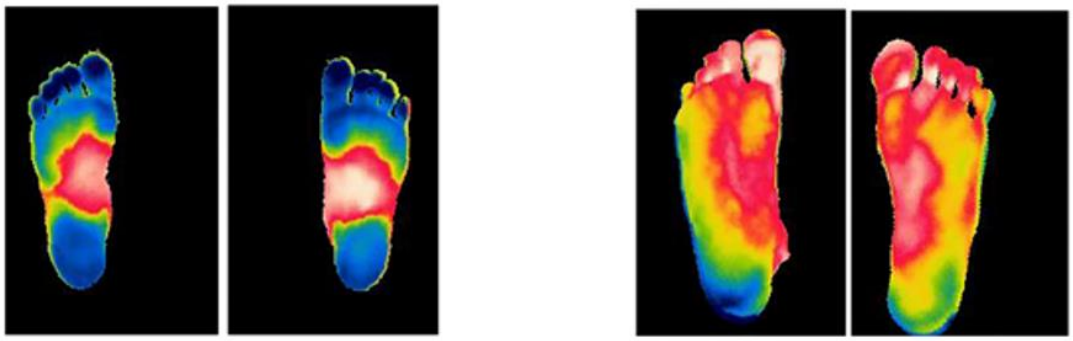

(a) (b)

Fig 2.17 Segmented Left and Right Foot Regions - (a) Control, (b) DM group [38]

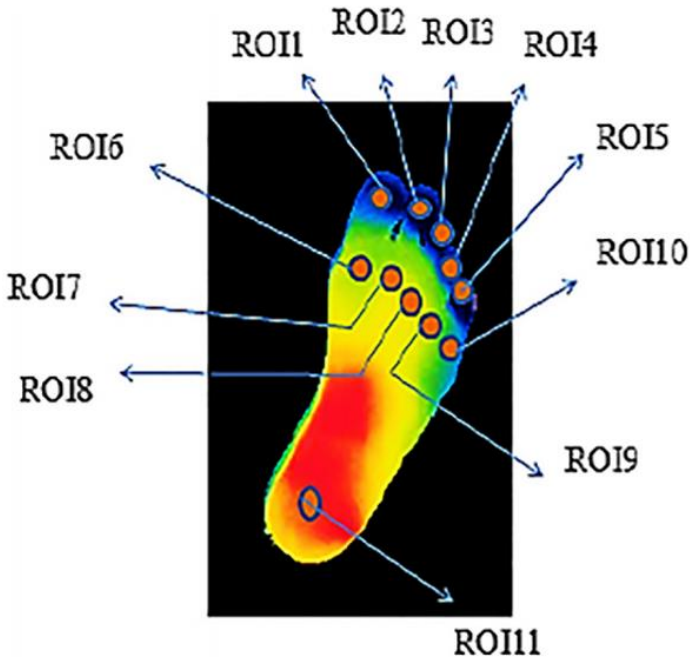

Fig 2.18 Primary regions 'at risk' for developing diabetic foot complications [38]

3) Merits and Demerits

Merits and demerits of the proposed algorithm are listed in Table 2.4 as depicted.

Table 2.4 Merits and Demerits of the Proposed Methodology

MERITS	DEMERITS
• Efficient algorithm for early detection of diabetic foot – uses asymmetry analysis of both texture and temperature features. • Performance achieved was significantly better than the other methods reported in the literature. • High accuracy	• Texture features essential for early identification of diabetic foot complications not combined – can promise earlier detection.

2.3.3 AlexNet and GoogleNet

Examining the usage of AI and DL for DF thermogram classification is the major objective of this paper [16]. GoogleNet and AlexNet (transfer learning algorithms) have been implemented. AlexNet is used for binary classification into CG and DM group thermographic images. GoogleNet is executed for classification into five levels based upon TCI values. DL and AI are being utilized as supplementary tools for help in diagnosing DFUs medically.

1) Procedure:

- **Thermal image acquisition:** From an openly available dataset [45]. 110 foot images (including CG and DM) are acquired.

- **Segmentation:** Methodology based on histogram characterized by fuzzy sets was implemented which is depicted in Fig 2.19.

- **Classification:** AlexNet; GoogleNet (DL algorithms. Specified parameters - minibatch size: 64; max. epochs: 100; solver: Adam, learning rate: 0.001. 30%: validation; 70%: training [16].

- **TCI (Thermal Change Index):** 5- level classification procedure based on TCI was used. It is the mean difference between equivalent DM group angiosomes and reference values attained from CG angiosomes [37]. It is represented in (2.6).

$$TCI = \frac{\sum |C_{ang} - DM_{ang}|}{4} \tag{2.6}$$

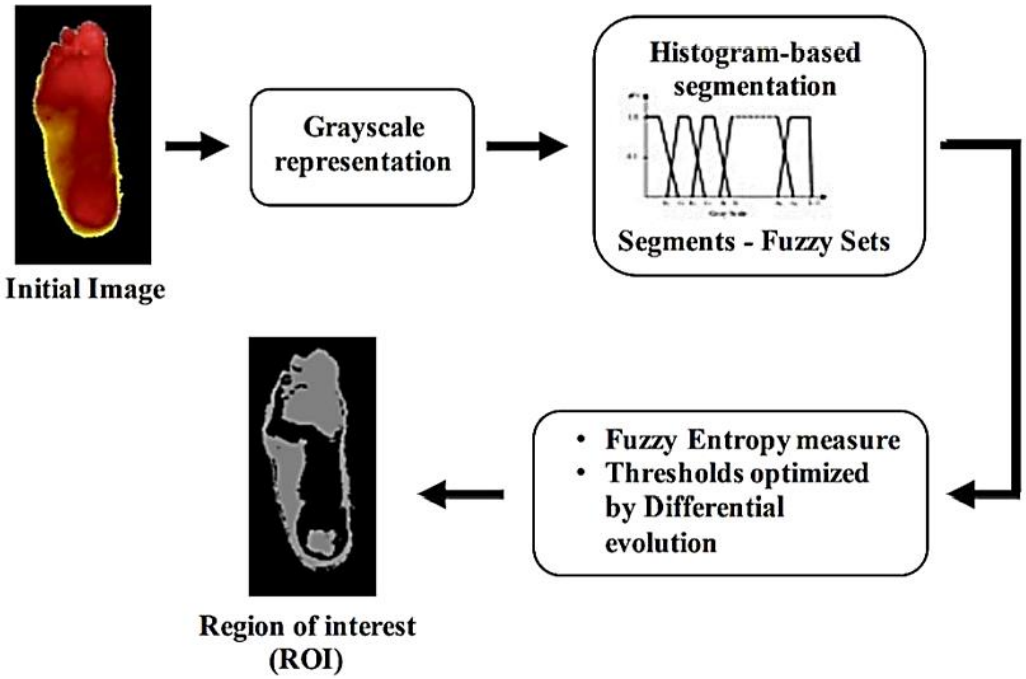

Fig 2.19 Automatic Segmentation Process [16]

(2) Results:

Pixel count, variance, mean, index grayscale value, and extreme value of entropy are contained in the feature vector obtained after extraction. It was a 5 category classification that denoted degree change in temperature of foot as depicted in Fig 2.21. Values of entropy for thresholds- two: 0.7810, three: 0.5269, four: 0.4572 [45]. Resultant value of sensitivity: 0.916 and accuracy: 0.853 is found in the methodology proposed. 1,2 and 4,5 cases had optimum results. Fig 2.20-2.21 illustrate the results.

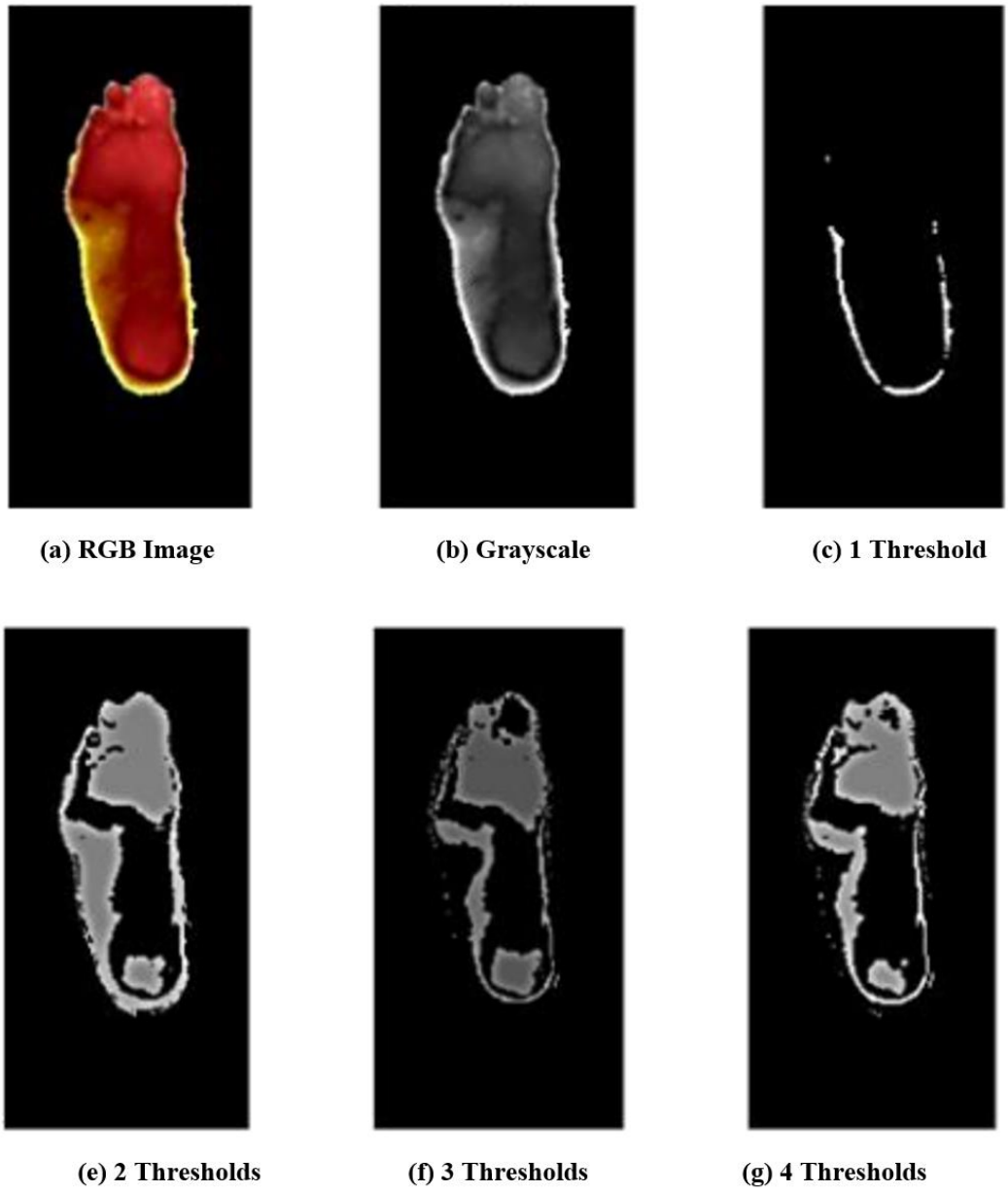

(a) RGB Image **(b) Grayscale** **(c) 1 Threshold**

(e) 2 Thresholds **(f) 3 Thresholds** **(g) 4 Thresholds**

Fig 2.20 Images of the Automatic Segmentation Process [16]

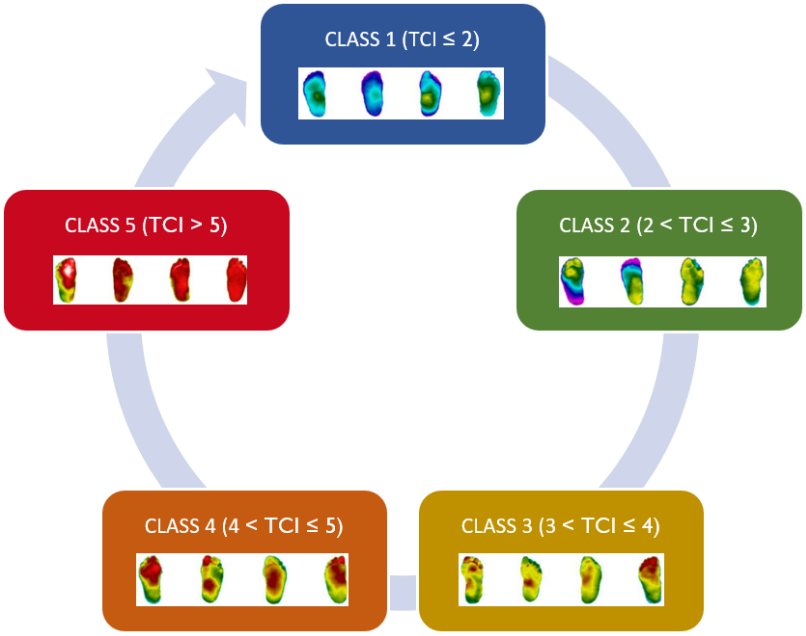

Fig 2.21 Classification of DFUs based on TCI value

3) Merits and Demerits:

Table 2.5 lists the pros and cons of the proposed techniques in the literature.

Table 2.5 Merits and Demerits of the Proposed Method

MERITS	DEMERITS
• TCI - an attempt to overcome differences in thermal pattern assumptions when both feet are compared. • Increase in the accuracy level in classification processes • Avoids the exhaustive task of feature extraction and segmentation of the desired patterns. • Low training time	• Requires a large amount training data • Pretrained networks do not work well if datasets are too difficult to classify • Not effective in classifying feet which contain quite distinctive texture and color features

2.3.4 Comparative Review of Classification Methodologies

Table 2.6 lists various ML techniques used in the literature along with the results.

Table 2.6 Comparison of Machine Learning Algorithms used in Literature

Research Work	Classification Technique	Accuracy (%)	Sensitivity (%)	Specificity (%)
Saminathan et. al [2020] [1]	SVM	91.23	91.50	92.41
Gururajarao et. al [2019] [2]	MobileNet	93.61	-	-
Cruz-Vega I et. al [2020] [3]	Binary Classification: AlexNet	94.57	92.67	93.77
	Multiclass Classification: GoogleNet	83.33	86.89	85.45

The key objective of this work is to do a comparative analysis of the performance of DL networks such as AlexNet, ResNet and proposed method, i.e., ProNet in detection as well as classification of DFUs with the help of foot thermograms. In the work proposed, there has been an attempt to optimize the DL network in the proposed method for attaining desirable performance in classification of foot thermographic images.

Although substantial work has been done in binary classification of DFUs, i.e.; into DM and CG, not many trials have been given to multiclass (multilevel) classification. Also, the foremost aim of this work is to comparatively examine the performance of transfer learning DL neural networks, DarkNet-19, DarkNet-53 and proposed novel network, i.e., Pro-Multi-Net in multilevel classification of DFUs by means of foot thermograms. In this work, an effort has been made to enhance the performance of DL networks by combining two algorithms to design the proposed network architecture. This is done for achieving better results than the reported works for multiclass DFU classification.

CHAPTER - 3

DEEP LEARNING TECHNIQUES

In this chapter, a detailed explanation of convolutional neural network which is a deep learning technique is provided along with its layers. Also, transfer learning approach involving pretrained deep neural networks is described. Furthermore, the techniques implemented in this work for binary classification and multiclass classification of diabetic foot thermograms are discussed including the novel and proposed methodology.

3.1 Convolutional Neural Network (CNN)

CNN is a DL algorithm that can input an image, allocate importance i.e.; learnable biases and weights to numerous objects in image and has ability to segregate them. CNNs require lower preprocessing than other methodologies for classification. With adequate training, CNNs are capable in learning the characteristics or filters, which on the other hand, in traditional techniques are hand engineered [46,47].

CNN architecture is similar to connectivity design of neurons in human brain. It was stimulated by the Visual Cortex association in which distinct neurons reply to inducements in restricted region of the visual (receptive) field. The whole visual area is covered by a group of these fields.

3.1.1 CNN Layers

The diverse layers in CNN as depicted in Fig are as follows:

1) **Input Layer:** It comprises image data which is represented by 3-D matrix.

2) **Convo Layer:** It is known as feature extractor layer because image features are extracted in this. To accomplish this operation, an image fragment is connected to this layer. Dot product b/w filter and receptive field is calculated. Single integer volume output is the operation result [46].

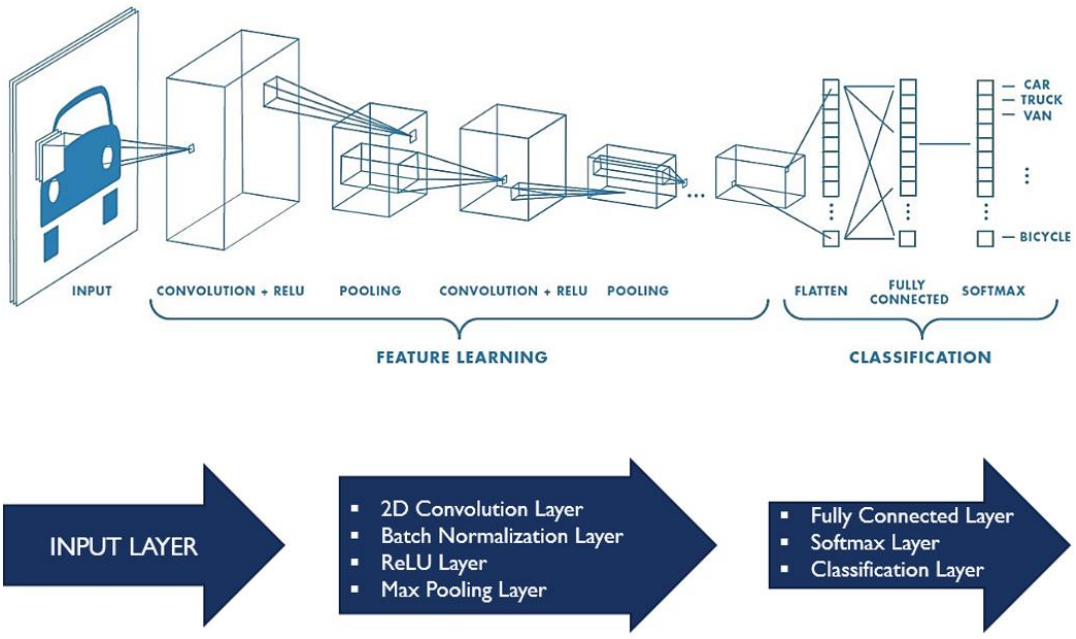

Fig 3.1 Feature Detection and Classification using CNN [9]

3) **Batch Normalization Layer:** Each layer of the network can learn with greater independence with this layer's help. The input layer is ascended by the activations in normalization. Also, it is utilized in normalizing the output of preceding layers.

4) **Pooling Layer:** It is used to decrease the 3-D volume of image input afterward convolution. If FC is applied next to Convo layer without max pooling, its affluent. Therefore, the only means to lessen the spatial volume of image that is input - max pooling.

5) **Fully Connected Layer:** FC includes biases, neurons and weights. Neurons in 1 layer are attached to that in another. It is utilized for classifying images amid diverse categories by training.

6) **Logistic (Softmax) Layer:** It exists at the end of FC layer. Softmax layer is used in multi-classification whereas logistic in binary classification.

7) **Output Layer:** This contains label in 1 hot encoding format.

3.2 Transfer Learning

Deep CNNs are pretrained to classify the different collection of images, which makes this process time efficient than the others. As this involves collecting learnt data from one model and implying that onto the next model, it is termed as transfer learning [48]. It is frequently used in DL applications. This approach is depicted in Fig 3.1.

Network training from scratch with arbitrarily set weights is a tedious task. Transfer learning makes fine-tuning of a network much easier and quicker. This is because it uses pretrained network as a preliminary point for learning a new job [49]. Learned features can be transferred to a new task with ease using lesser training images.

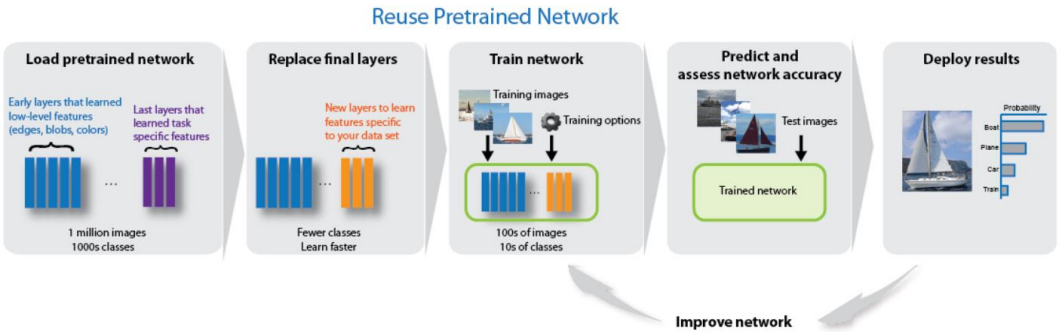

Fig 3.2 Transfer Learning [9]

3.3 Binary Classification Algorithms

For binary classification into CG and DM groups, methodologies implemented in this work are AlexNet and Resnet-101. Advantageous features of both these networks are then combined to design ProNet, the proposed DL network which will be discussed in this section along with the other two algorithms.

3.3.1 AlexNet

As shown in Fig 3.3, overall, 5 convolutional layers (CL) make up this network which had 3 pooling layers in it, a soft max layer (having output classes as 2), and 2 FLCs (fully connected layers) [50]. Input image has the dimension as 227×227×3. In this, the input image with kernels are transformed by CL, every kernel being sized at 11×11×3. These are treated in 4 phases or strides which act as input to next layer.

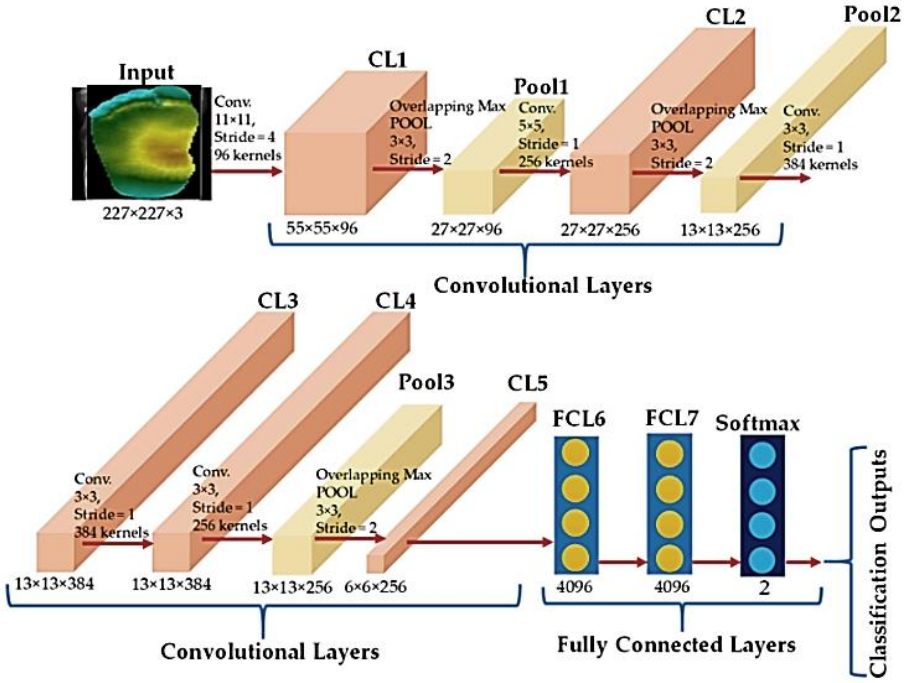

Fig 3.3 Architecture of AlexNet

3.3.2 ResNet-101

As the name signifies, this algorithm consists of residual network for improving transmission of features. This happens because of a shortcut connection into CNN. It is designed by connecting numerous residual blocks [51]. Addition of shortcut in every two convolutional layers constitutes such blocks. After a point, accuracy saturates and then declines rapidly because of increasing depth while training DL networks. For combating this issue (also known as 'degradation problem'), residual (identity) mapping method is used by ResNet. Some of the weighted layers may not fit in the desired mapping directly. So, framework of this network enables such layers to fit in an identity mapping [53].

Fig 3.4 depicts a building block of ResNet. 'x' denotes the network input. The output of the two convolution layers is represented by F(x). The original output is overlaid with rapid connection mapping $(F(x) + x)$. This leads to a reduction in network training complexity and increase in accuracy.

Different kinds of building blocks of this network is shown by Fig 3.5. Resnet-101 is comprised of 101 layers and the dimensions of the input image are 224×224×3.

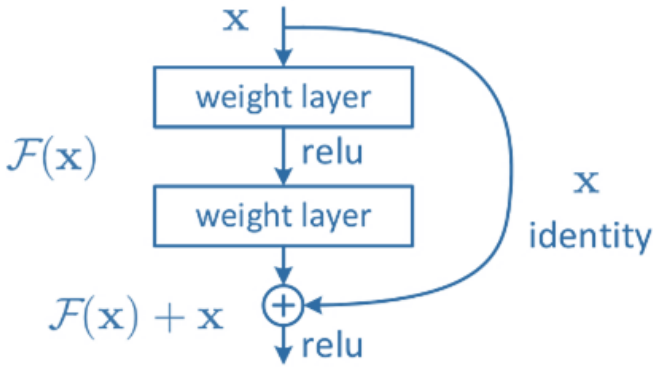

Fig 3.4 Building Block in ResNet

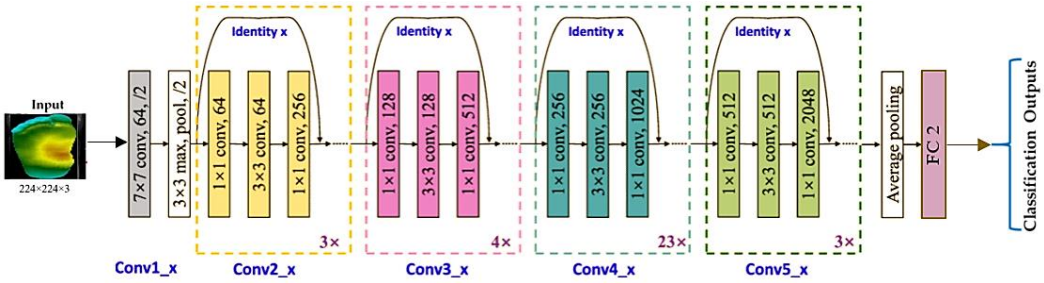

Fig 3.5 ResNet-101 Architecture

3.3.3 Proposed Methodology

The proposed deep CNN, named as ProNet, combines the best features of both AlexNet and ResNet-101. The number of layers are reduced in ProNet as in AlexNet (having lesser layers). It has a similar architecture to ResNet-101. The designed network has 66 layers as compared to 101 layers (in ResNet-101) for a decrement in network complexity and training time. Dropout layers are added to reduce overfitting.

As depicted in Table 3.1, one dropout layer (of probability 0.5) is inserted in each of the convolution blocks i.e., Conv2_x, Conv3_x, Conv4_x and Conv5_x. Therefore, it sums upto 16 dropout layers in the entire network (Conv_2: 3×1; Conv_3: 4×1; Conv_4: 6×1; Conv_5: 3×1). FC layer, connected after average pooling layer, has output classes specified as 2 (CG and DM groups). Also, training parameters are fine tuned for performance optimization. Fig 3.6. provides a detailed depiction of network architecture of ProNet.

Table 3.1 Convolution Block Framework in ProNet

CONVOLUTION BLOCK	LAYER COUNT	OUTPUT SIZE	FILTER SIZE	FILTER COUNT	STRIDE
Conv1_x	2	112 × 112	7 × 7	64	2
		Max Pooling layer (Pool Size: 3 × 3; Stride: 2)			
Conv2_x	12 (3 × 4)	56 × 56	1 × 1	64	1
		56 × 56	3 × 1	64	1
		Dropout layer (Probability: 0.5)			
		56 × 56	1 × 1	256	1
Conv3_x	16 (4 × 4)	28 × 28	1 × 1	128	1
		28 × 28	3 × 1	128	1
		Dropout layer (Probability: 0.5)			
		28 × 28	1 × 1	512	1
Conv4_x	24 (6 × 4)	14 × 14	1 × 1	256	1
		14 × 14	3 × 1	256	1
		Dropout layer (Probability: 0.5)			
		14 × 14	1 × 1	1024	1
Conv5_x	12 (3 × 4)	7 × 7	1 × 1	512	1
		7 × 7	3 × 1	512	1
		Dropout layer (Probability: 0.5)			
		7 × 7	1 × 1	2048	1
Total number of Layers: 66					

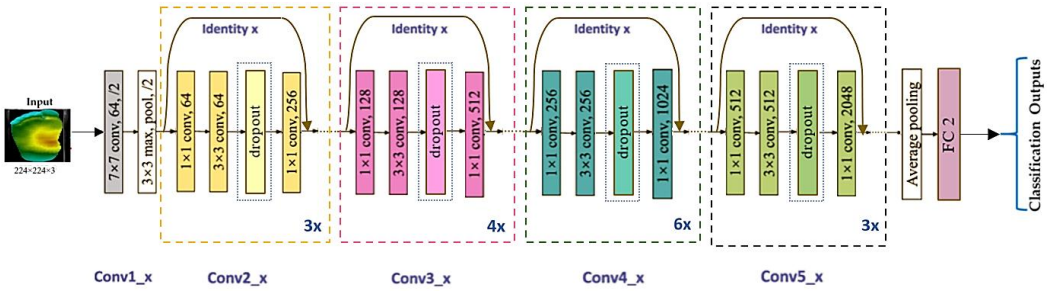

Fig 3.6 Architecture of ProNet

3.4 Multiclass Classification Algorithms

For multiclass classification of foot thermograms into 5 classes based on TCI values, valuable features of two networks – DarkNet-19 and DarkNet-53 are used to design Pro-Multi-Net, the proposed technique. All the three algorithms implemented are illustrated and discusses in detail in this section.

3.4.1 DarkNet-19

Input image to this network has dimension as 256×256×3. As depicted in Fig 3.7 (a), 19 convolutional layers (CLs) make up DarkNet-19, in addition to which there

are 5 max-pooling layers. Filter sizes of convolutional and max pooling layers (of stride 2) are specified in the figure. For compressing depiction of features between 3×3 convolutions, it uses 1×1 filters and global average pooling layer for making predictions. the network consists of one FLC (fully connected layer) and 5 output classes [53].

3.4.2 DarkNet-53

As the name indicates, DarkNet-53 comprises of 53 convolutional layers [54]. The network uses these 53 CLs. Fig 3.7 (b) depicts the architecture of this methodology. There are 5 convolutional blocks (conv_1x to conv_5x) consisting of successive 3×3 and 1×1 CLs. Moreover, there is a max pooling layer and a residual layer in each block. This residual layer acts as a skip connection that helps in enhancing feature transmission [55]. Because of this, there is propagation of activations deeper into the layers. And this happens without degradation of the gradient. Size of the DFU thermogram input is 256×256×3.

3.4.3 Proposed Technique

Pro-Multi-Net, the proposed innovative method combines the optimal features of both DarkNet-19 and DarkNet-53. Pro-Multi-Net has minimized number of as in DarkNet-19. The architecture of this algorithm is similar to DarkNet-53. There are 33 CLs in the network designed in contrast to 53 CLs (in DarkNet-53). This leads to a diminished in training time and also network complexity.

Overfitting is reduced by insertion of one dropout layer of ½ probability every convolution block (conv_1x: conv_5x). Thus, 9 dropout layers are there in the entire network (conv_1x - 1×1; conv_2x - 2×1; conv_3x - 4×1; conv_4x - 4×1; conv_5x - 2×1). Furthermore, global average pooling layer and FC are connected and output classes are taken as 5. In addition to this, to attain optimized performance, training metrics are fine tuned. Fig 3.7 (c) shows the architecture of Pro-Multi-Net in detail. Table 3.2 describes the framework of all the convolution blocks in Pro-Multi-Net.

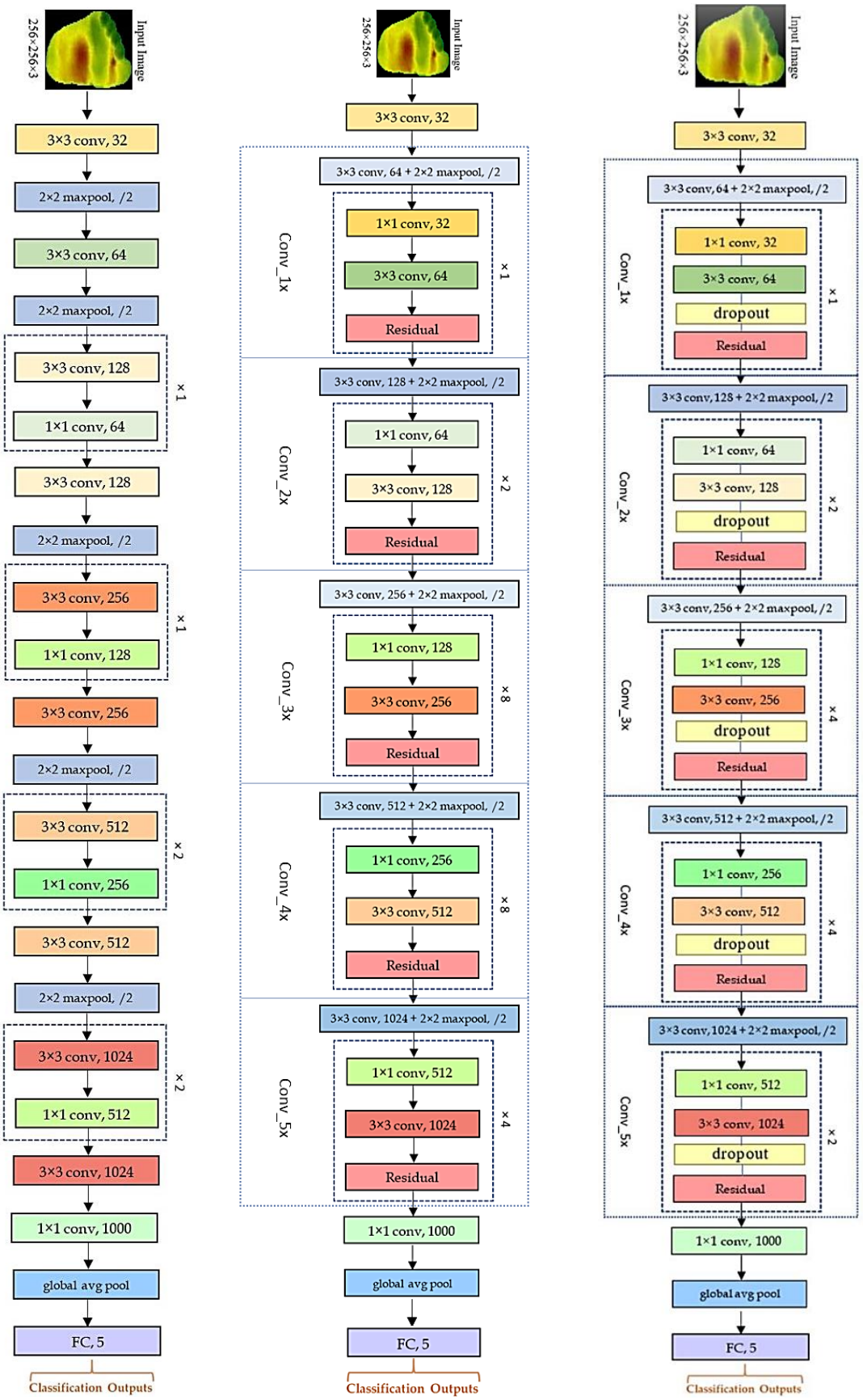

Fig 3.7 Architecture of (a) DarkNet-19; (b) DarkNet-53 and (c) Pro-Multi-Net

Table 3.2 Convolution Block Description in Pro-Multi-Net

CONVOLUTION BLOCK	CONVOLUTIONAL LAYER COUNT	OUTPUT SIZE	FILTER SIZE	FILTER COUNT	STRIDE
Layer 1	1	256 × 256	3 × 3	32	1
conv1_x	3 (1 + (1 × 2))	128 × 128	3 × 3	64	2
		Max Pooling (Pool Size: 2 × 2; Stride: 2)			
		128 × 128	1 × 1	32	1
		128 × 128	3 × 3	64	1
		Dropout (Probability: 1/2)			
		Residual			
conv2_x	5 (1 + (2 × 2))	64 × 64	3 × 3	128	2
		Max Pooling (Pool Size: 2 × 2; Stride: 2)			
		64 × 64	1 × 1	64	1
		64 × 64	3 × 3	128	1
		Dropout (Probability: 1/2)			
		Residual			
conv3_x	9 (1 + (4 × 2))	32 × 32	3 × 3	256	2
		Max Pooling (Pool Size: 2 × 2; Stride: 2)			
		32 × 32	1 × 1	128	1
		32 × 32	3 × 3	256	1
		Dropout (Probability: 1/2)			
		Residual			
conv4_x	9 (1 + (4 × 2))	16 × 16	3 × 3	512	2
		Max Pooling (Pool Size: 2 × 2; Stride: 2)			
		16 × 16	1 × 1	256	1
		16 × 16	3 × 3	512	1
		Dropout layer (Probability: 1/2)			
		Residual			
conv5_x	5 (1 + (2 × 2))	8 × 8	3 × 3	1024	2
		Max Pooling (Pool Size: 2 × 2; Stride: 2)			
		8 × 8	1 × 1	512	1
		8 × 8	3 × 3	1024	1
		Dropout layer (Probability: 1/2)			
		Residual			
Layer 33	1	8 × 8	1 × 1	1000	1
	Total Convolutional Layers = 33				

Simulation details along with the results will be provided in the following chapter. Also, all the methodologies implemented will be analyzed comparatively.

CHAPTER - 4

RESULTS AND DISCUSSION

This chapter explains the software tool utilized to implement all the techniques in this work. Also, the dataset used, training parameters, performance metrics and results obtained for binary and multiclassification of diabetic foot ulcer are discussed in detail. Also, comparative analysis of all the frameworks is provided.

4.1 Software Tool

All simulations are performed using MATLAB R2020a software. MathWorks developed MATLAB (MATrix-LABoratory), an exclusive and numeric computation setting [56]. It permits data and function plotting, algorithm simulation, manipulation of matrices, multilinguistic program interfacing and user interface creation.

For generating scripts combining output, code and configured text in a notebook, which is practicable, MATLAB comprises of Live Editor [57]. In it, a desktop setting adjusted for design procedures and reiterative study is combined together with programming language which directly explains mathematics of arrays and matrices.

Toolbox is a feature set through which helps MATLAB in expansion of its advances and functions of all disciplines. There are a diversity of toolboxes as contained in MATLAB such as statistics and ML toolbox (for analysis of model data using ML and numbers), DL toolbox (used in training, designing and interpretation of DL networks) [58].

4.1.1 Deep Network Designer

All the networks are implemented using Deep-Network-Designer app, a feature of DL toolbox of MATLAB software. It helps in visualizing, building and training DL networks collaboratively [59].

The primary features of this app include:

1) Importing, building, editing and combining of ML and DL networks.

2) Adding of new layer connections and editing and viewing layer features.

3) For transfer learning, loading and editing pretrained networks.

4) By diagnosing complications prior to training and safeguarding the correctness of network architecture definition, it helps in framework analysis.

5) Visualizing class label distribution and augmenting image categorization training dataset.

6) Envisioning and importing image data and datastores for validating and training.

7) Training of networks and monitoring the training by plotting loss, accuracy and validation parameters.

8) Utilizing Experiment Manager for creating experimentations for tuning of hyperparameters.

9) Generating code in MATLAB to train and build network frameworks.

10) Exporting trained networks to Simulink or workspace.

4.2 Binary Classification Results

This section gives a description of the dataset, training metrics, performance parameters and experimental results for DFU thermogram binary classification methods implemented in this work.

4.2.1 Dataset

Foot thermograms are obtained from IEEE Dataport [45] for two categories. Control Group (CG) consists of feet thermograms of those people which have minor risk of ulceration whereas persons in DM (Diabetic Mellitus) group have greater chances of DFU.

In CG, there are thermographic feet images of 45 people (total images: 90 (left & right foot)). DM group contains thermograms of 50 persons (total images: 100). Therefore, in total, there are 190 images. Out of these, 95 images are used for testing purposes.

4.2.2 Training Parameters

Training input parameters that are used in this work, as listed in Table 4.1 are described as:

1) **Solver:** SGDM (Stochastic-Gradient-Descent-with-Momentum) solver is a technique that aids in enhancing gradient vectors in correct directions [60]. Quicker convergence is the result of this. It is amongst major prevalent algorithms for optimization purposes and a lot of models are trained with its help.

2) **Maximum epochs:** An epoch designates that the no. of passes of complete dataset training by ML methodology has finished. If data amount is extremely huge, databases are generally congregated into batches.

3) **Initial Learn Rate:** It is a hyperparameter (configurable) utilized in neural network training. Its value lies between 0 and 1 (a little positive value). It controls the adaptability of the model to situation.

4) **Mini Batch Size:** Before updation of the internal parameters of model, a number of samples are there which have to be worked through. This number is denoted by mini batch size.

Table 4.1 Training Input Parameter Specifications

TRAINING PARAMETER	DEEP NEURAL NETWORK		
	AlexNet	***ResNet-101***	***ProNet***
Input Image Size	227×227×3	224×224×3	224×224×3
Solver	SGDM	SGDM	SGDM
Maximum epochs	30	10	10
Mini Batch Size	128	10	10
Initial Learn Rate	1E-4	1E-3	3E-3

4.2.3 Performance Metrics

The performance metrics for all the three methodologies (AlexNet, Resnet101 and ProNet) i.e., confusion matrix, accuracy, precision, sensitivity, specificity and F1-score are as follows:

1) **Confusion Matrix:** It is an N×N matrix that is utilized for assessment of performance of classification technique as shown by Fig 4.1. N is the no. of target groups. Confusion matrix compares the projected target values obtained by DL model to the actual target class values [61].

2) **Accuracy:** It is the ratio of correct predictions to total predictions made for a dataset as depicted in (4.1). Here, TP: no. of true positives; TN: no. of true negatives; FN: no. of false negatives and FP: no. of false positives.

$$Accuracy = \frac{TP+TN}{TP+FN+TN+FP} \tag{4.1}$$

3) **Precision:** It is a parameter which measures the no. of right positive predictions. It is formulated as the ratio of rightly predicted positives to the total positive examples predicted as in (4.2).

$$Precision = \frac{TP}{TP+FP} \tag{4.2}$$

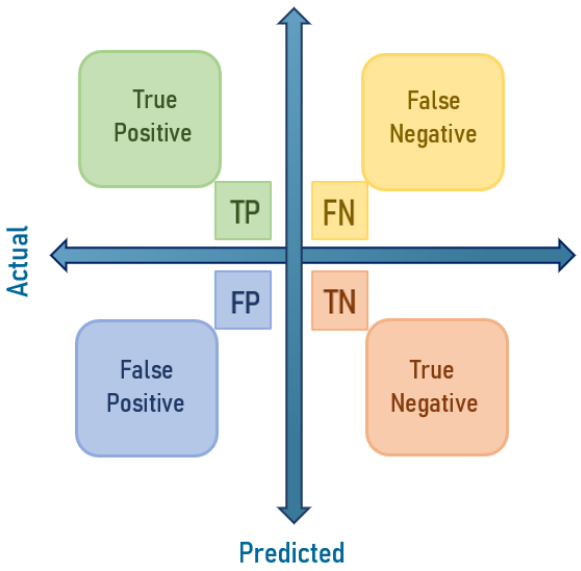

Fig 4.1 Confusion Matrix for Binary Classification

4) **Sensitivity:** It is a parameter that computes correct positive estimates of all positive examples which could have been predicted. It is equated as the ratio of TPs to the total TPs and FNs as represented in (4.3).

$$Sensitivity = \frac{TP}{TP+FN} \tag{4.3}$$

5) **Specificity:** It is the quantity of real negatives, that are also forecasted as negative. It is equated as the ratio of TNs to the total TNs and FNs as shown in (4.4).

$$Specificity = \frac{TN}{TN+FP} \tag{4.4}$$

6) **F1-Score:** It provides a method to combine both sensitivity and precision into a sole measure which has both the properties. It is harmonic mean of two fractions as given by (4.5).

$$F1 - Score = 2 * \frac{(Precision * Sensitivity)}{(Precision + Sensitivity)} \tag{4.5}$$

4.2.4 Result Analysis

An overview of the training time taken by all three DL techniques implemented is given in Table 4.2. It can be observed that if the time taken by AlexNet is denoted by 't', ResNet-101 takes seven times the time consumed by training AlexNet. ProNet, the proposed network, consumes four times the time. AlexNet consumes minimum training time due to least number of layers but also has the lowest accuracy. ProNet, proposed network takes more time for training than AlexNet. But, it is less complex and tedious than ResNet because of reduction in the number of layers.

Table 4.2 Training Time Observations

DEEP NEURAL NETWORK	TRAINING TIME
AlexNet	t
ResNet-101	7t
ProNet	4t

Fig 4.2 (a)-(c) depict testing output samples (of diabetic foot thermograms) of AlexNet, ResNet-101 and ProNet with their prediction probability percentages. Control Group sample is denoted by ‘cg’ and that of Diabetes Mellitus group is represented by ‘dm’.

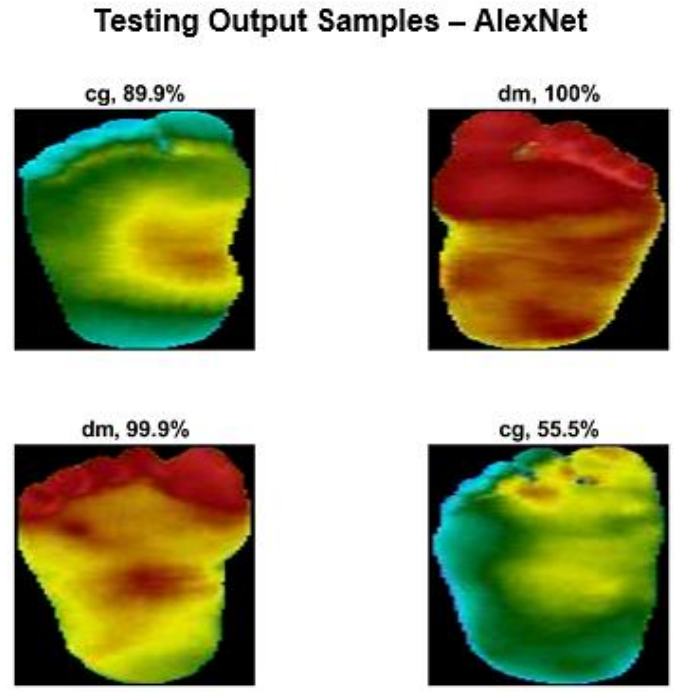

(a)

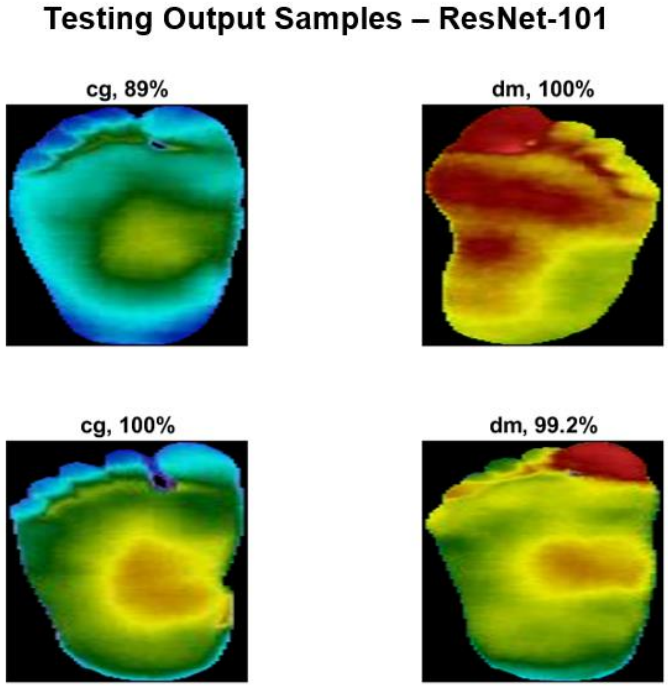

(b)

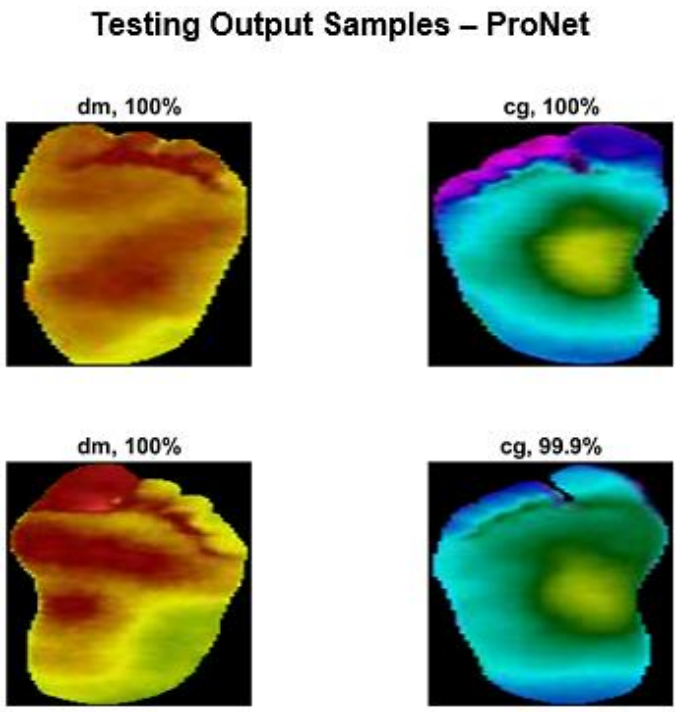

(c)

Fig 4.2 Testing Output Samples for (a) AlexNet; (b) ResNet-101; (c) ProNet

It can be observed that two out of every four samples tested have 100% probability of being predicted correctly in case of AlexNet and ResNet-101. The rest two samples have a higher percentage of being predicted incorrectly by AlexNet than by ResNet-101. In case of ProNet, three out of every four samples have complete chances of correct estimate. Only one out of every four samples has probability of being predicted slightly inaccurately (as small as 0.1%).

Confusion matrices obtained for the methods implemented are shown in Fig 4.3 (a)-(c). The matrices depict the number of TPs, FNs, FPs and TNs along with prediction percentages for each class – CG and DM. Also, percentage accuracy is represented for each DL technique.

The values for all performance parameters are calculated as recorded in Table 4.3. It can be observed from Table 4.3 that AlexNet has greater accuracy (96.8%) than that of classification models in the previously reported work [5,6,8].

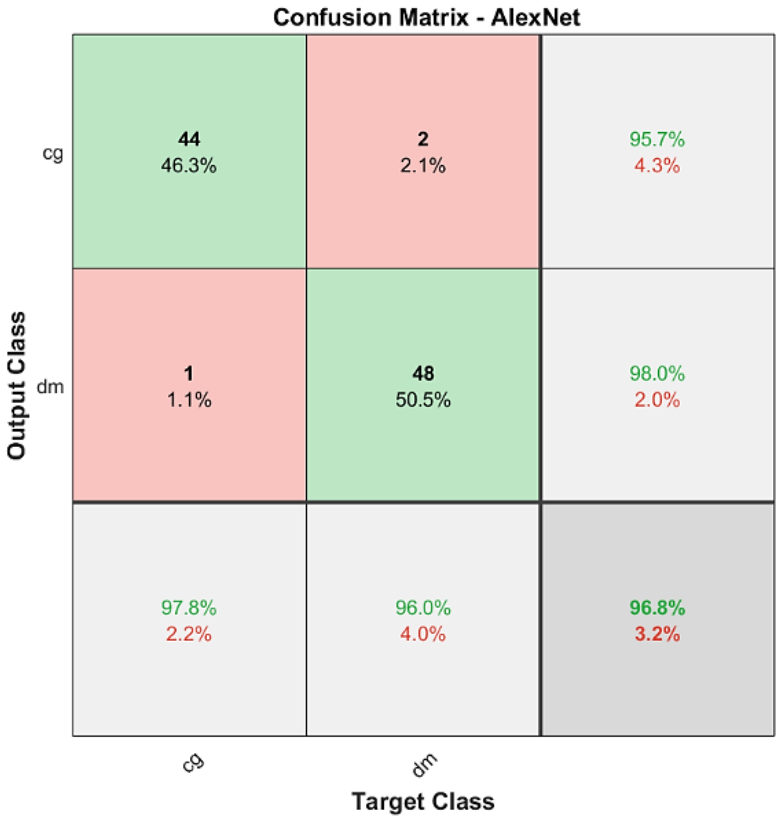
Confusion Matrix - AlexNet
cg
dm
Output Class
44
46.3%
2
2.1%
95.7%
4.3%
1
1.1%
48
50.5%
98.0%
2.0%
97.8%
2.2%
96.0%
4.0%
96.8%
3.2%
cg
dm
Target Class

(a)

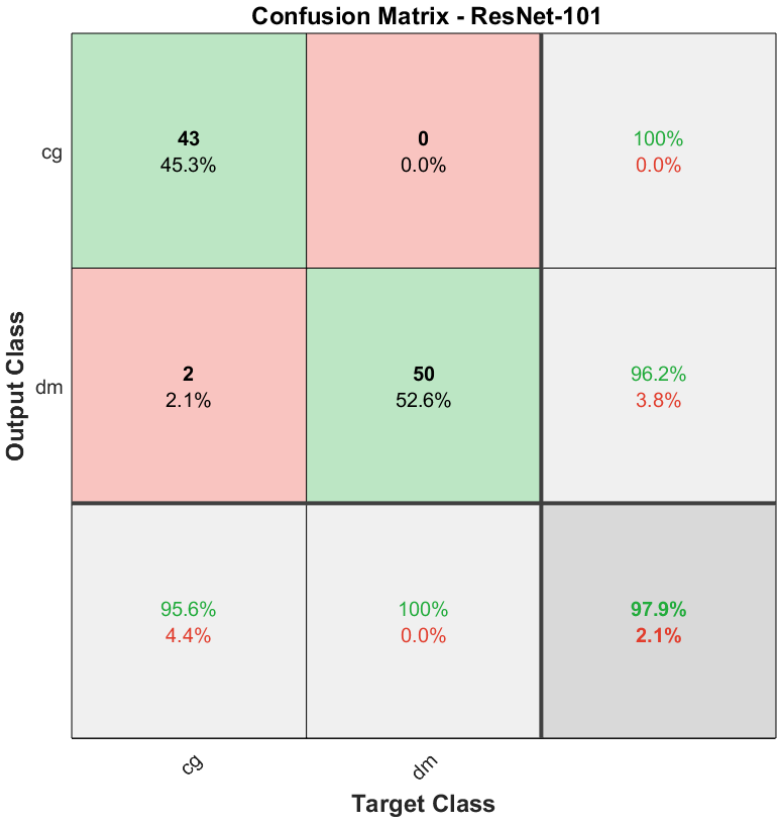
Confusion Matrix - ResNet-101
cg
dm
Output Class
43
45.3%
0
0.0%
100%
0.0%
2
2.1%
50
52.6%
96.2%
3.8%
95.6%
4.4%
100%
0.0%
97.9%
2.1%
cg
dm
Target Class

(b)

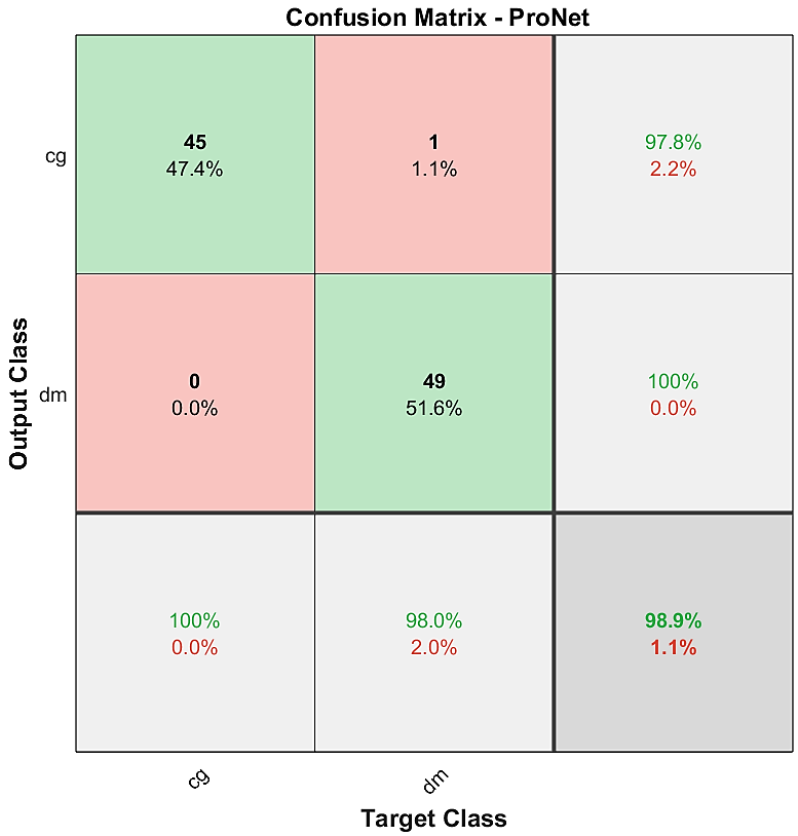

(c)

Fig 4.3 Confusion Matrix for (a) AlexNet; (b) ResNet-101; (c) ProNet

Table 4.3 Performance Metric Calculations

PERFORMANCE METRIC	DEEP NEURAL NETWORK		
	AlexNet	***ResNet-101***	***ProNet***
Accuracy	0.968	0.979	0.989
Precision	0.956	0.955	1.000
Sensitivity	0.977	1.000	0.978
Specificity	0.960	0.962	1.000
F1 Score	0.966	0.976	0.988

Although ResNet-101 has higher values than AlexNet for most of the metrics, it has lower accuracy, precision, specificity and F1-Score than the DL network proposed in this work. Except for the fact that ProNet has lower sensitivity than ResNet-101 (which has a perfect sensitivity value of 1), it gives the best results amongst the other two in terms of accuracy (as high as 98.9%) and all other parameter values. Also, it has optimal precision and specificity.

4.3 Multiclass Classification Results

This section gives a description of the dataset, training metrics, performance parameters and experimental results for DFU thermogram binary classification methods implemented in this work.

4.3.1 Dataset

Diabetic foot thermograms are collected from the database of IEEE Dataport [45]. It consists of 190 foot thermograms of CG and DM groups combinedly. Also, TCI value is specified for each thermographic image.

The dataset is segregated into 5 classes as per TCIs described in [5]. There are 38 images in each class. Out of the total thermograms, 110 are used for testing (22 for each class). As shown by Fig 6., classes based on TCI ranges are stated as follows:

1) **Class 1 (TCI ≤ 2):**

   It is the reference value taken for abnormality indication.

2) **Class 2 (2 < TCI ≤ 3):**

   As TCI increments, foot thermograms belonging to class 2 are differentiated by the loss of the butterfly pattern.

3) **Class 3 (3 < TCI ≤ 4):**

   In this class, foot thermograms have bigger hot regions in support points which can also spread through the heel.

4) **Class 4 (4 < TCI ≤ 5):**

   It contains high temperature regions compared to class 3.

5) **Class 5 (TCI > 5):**

   In this class, hot area covers almost the complete sole.

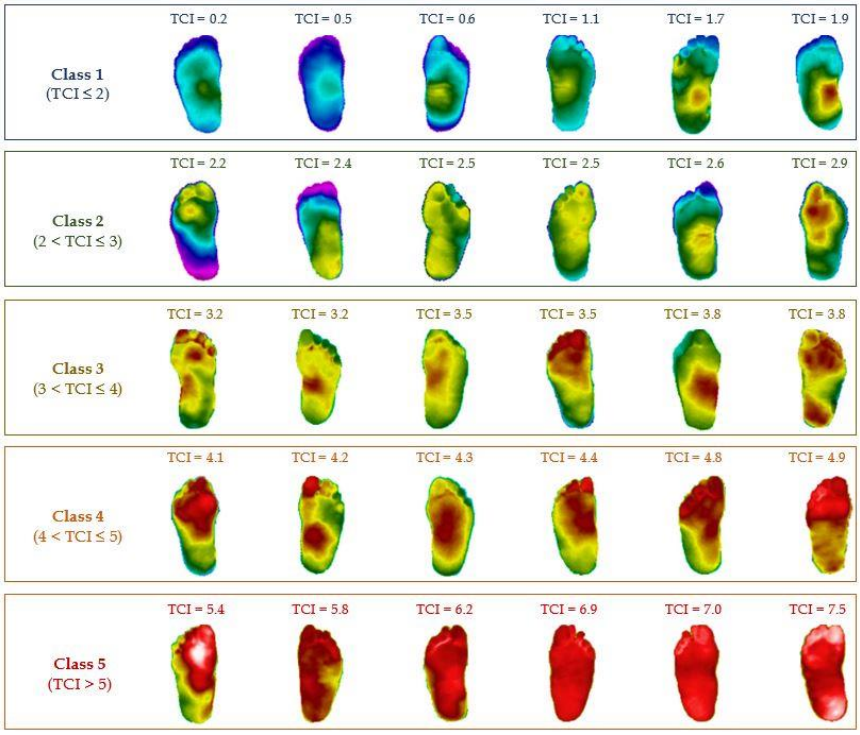

Fig 4.4 TCI Ranges for Five Classes of Foot Thermograms

4.3.2 Training Parameters

Training parameters that are specified in this work, as listed in Table 4.4 are defined as:

1) **Input Image Size:**

   As specified in the table, input thermogram image size for all the algorithms applied is 256×256×3.

2) **Solver:**

   For the enhancement of gradient vectors in accurate directions, the solver method used is SGDM (Stochastic-Gradient-Descent-with-Momentum). Several DL models are trained with this solver as it leads to earlier convergence. It is one of the key optimization techniques used [62].

3) **Initial Learn Rate:**

   For training DL networks, hyperparameter used is the learn rate. It is configurable and its value exists in the range (0,1). This has the capability of controlling model adaptability to the situation.

Table 4.4 Training Input Parameter Specifications

TRAINING PARAMETER	DEEP NEURAL NETWORK		
	DarkNet-19	***DarkNet-53***	***Pro-Multi-Net***
Input Image Size	256×256×3	256×256×3	256×256×3
Solver	SGDM	SGDM	SGDM
Initial Learn Rate	2E-4	1E-3	2E-3
Maximum epochs	20	10	10
Mini Batch Size	30	10	10

4) Maximum epochs:

Number of passes in training the entire dataset by the DL technique is denoted as epoch. The dataset is assembled into batches if the amount of data is large.

5) Mini Batch Size:

The number of sample images to be worked upon before internal parameters of method are up to date is indicated by mini batch size.

4.3.3 Performance Metrics

For all three algorithms (DarkNet-19, DarkNet-53 and Pro-Multi-Net), the performance parameters i.e., confusion matrix, accuracy, precision, recall and F1-score are as listed:

1) Confusion Matrix:

Fig 4.5 depicts confusion matrix (n x n) for multiclass classification. Observations that are correctly classified are represented (in terms of number of percentage) by diagonal cells. Whereas the incorrect classification observations are shown by off – diagonal elements [63].

'A' denotes the overall accuracy of the methodology implemented. The distant right column gives the recall percentages for all classes (C_1 to C_n). And the bottom row shows the precision percentages.

		Predicted (Target) Class				
Actual (Output) Class		C_1	C_2	$\cdots$	C_n	
	C_1	M_{11}	M_{12}	$\cdots$	M_{1n}	$R(C_1)$
	C_2	M_{21}	M_{22}	$\cdots$	M_{2n}	$R(C_2)$
	$\vdots$	$\vdots$	$\vdots$	$\vdots$	$\vdots$	$\vdots$
	C_n	M_{n1}	M_{n2}	$\cdots$	M_{nn}	$R(C_n)$
		$P(C_1)$	$P(C_2)$	$\cdots$	$P(C_n)$	A

Fig 4.5 Multiclass Classification Confusion Matrix

2) Accuracy:

The percentage of correct estimates to total predictions is represented by accuracy. For a multilevel classification, overall accuracy is also the summation of percentages denoted by diagonal elements (for each class) [64].

3) Precision:

It is known as the percentage of all samples predicted to be belonging to every class that are correctly classified [65]. As described in Fig 4.5, precision value is represented by (4.6) as:

$$P(C_n) = \frac{M_{nn}}{\sum_j M_{nj}} \tag{4.6}$$

where 'n' denotes the classification level, 'M' is the element, and 'j' represents the predicted (target) class number.

4) Recall:

The percentage of correctly classified samples for each class is called as recall [65]. As in Fig 4., recall value is formulated in (4.7) as

$$R(C_n) = \frac{M_{nn}}{\sum_j M_{jn}} \tag{4.7}$$

where 'n' represents the classification level for element 'M', and 'j' denotes the actual (output) class number.

5) F1-Score:

It is a combination of both recall and precision into a single measure. F1-Score is a harmonic mean of these two parameters as given by (4.8).

$$F1 - Score = 2 * \frac{(Precision * Recall)}{(Precision + Recall)} \quad (4.8)$$

4.3.4 Result Analysis

The training time consumption for all methods is shown in in Table 4.5. If the time consumed by DarkNet-19 is designated by 'τ', DarkNet-53 takes 2.5 times the time expended in training DarkNet-19. The proposed network, Pro-Multi-Net takes 1.5 times the time. Although, because of minimal number of layers, DarkNet-19 takes lowest time for training but also is the least accurate. Even though Pro-Multi-Net takes higher training time than DarkNet-19, due to condensed layers, it is less tedious than DarkNet-53.

Fig 4.6 (a)-(c) show the testing DFU thermogram testing output samples of DarkNet-19, DarkNet-53 and Pro-Multi-Net. The probability percentages of prediction for each class are also denoted along with. It can be observed that average percentage for correct prediction of every two samples increases as we move from DarkNet-19 to Pro-Multi-Net. Also, classes 1 and 5 have the highest correct prediction probabilities for each technique. Class 3 has the lowest percentage for accurate prediction.

Confusion matrices obtained after multilevel classification by the three networks are depicted in Fig 4.6 (a)-(c). The overall accuracy, precision and recall percentages are depicted as discussed previously in Section 4.3.3. Also error percentages are indicated for each class and performance metric below these percentages.

Table 4.5 Observed Training Time

DEEP NEURAL NETWORK	TRAINING TIME
DarkNet-19	τ
DarkNet-53	2.5 τ
Pro-Multi-Net	1.5 τ

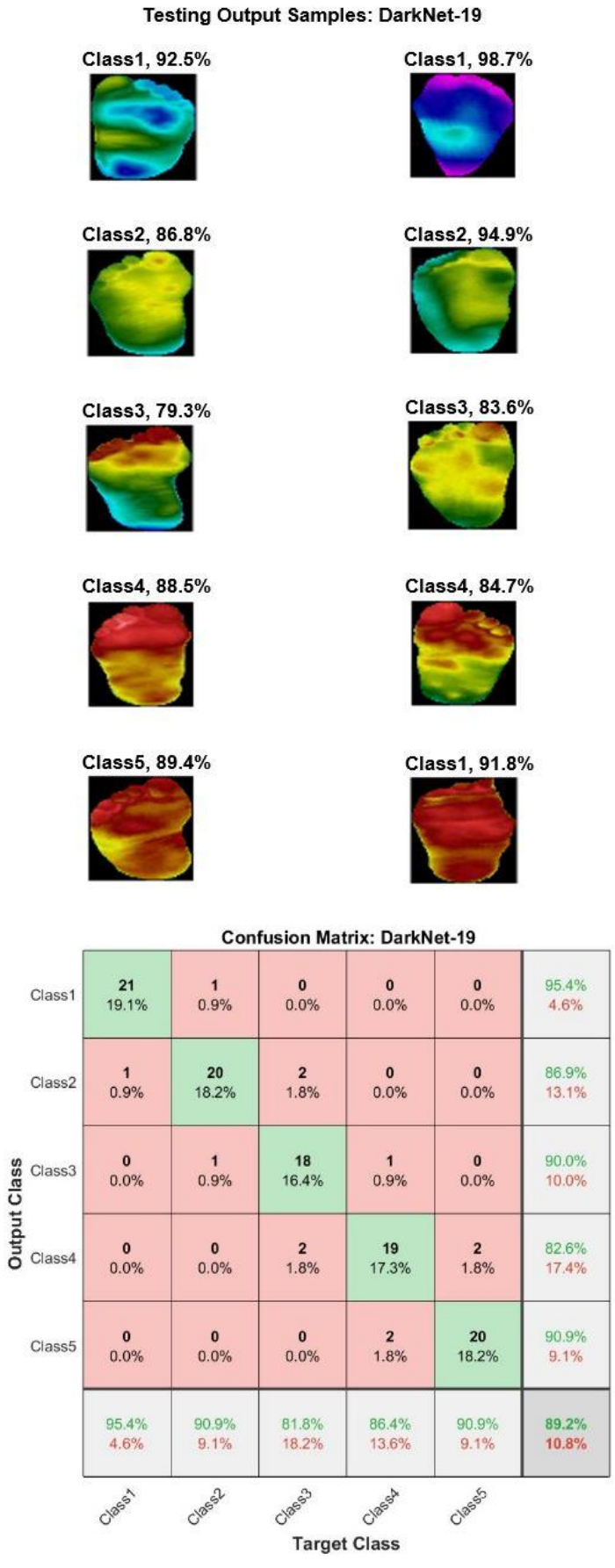
Testing Output Samples: DarkNet-19
Class1, 92.5%
Class1, 98.7%
Class2, 86.8%
Class2, 94.9%
Class3, 79.3%
Class3, 83.6%
Class4, 88.5%
Class4, 84.7%
Class5, 89.4%
Class1, 91.8%
Confusion Matrix: DarkNet-19
Output Class
Target Class
Class1
Class2
Class3
Class4
Class5
21 19.1%
1 0.9%
0 0.0%
0 0.0%
0 0.0%
95.4% 4.6%
1 0.9%
20 18.2%
2 1.8%
0 0.0%
0 0.0%
86.9% 13.1%
0 0.0%
1 0.9%
18 16.4%
1 0.9%
0 0.0%
90.0% 10.0%
0 0.0%
0 0.0%
2 1.8%
19 17.3%
2 1.8%
82.6% 17.4%
0 0.0%
0 0.0%
0 0.0%
2 1.8%
20 18.2%
90.9% 9.1%
95.4% 4.6%
90.9% 9.1%
81.8% 18.2%
86.4% 13.6%
90.9% 9.1%
89.2% 10.8%

(a)


Testing Output Samples: DarkNet-53
Class1, 100%
Class1, 99.9%
Class2, 94.3%
Class2, 86.7%
Class3, 82.9%
Class3, 89.5%
Class4, 88.7%
Class4, 93.9%
Class5, 93.8%
Class5, 97.9%
Confusion Matrix: DarkNet-53
Output Class
Target Class
Class1
Class2
Class3
Class4
Class5
22 20.0%
1 0.9%
0 0.0%
0 0.0%
0 0.0%
95.6% 4.4%
0 0.0%
20 18.2%
2 1.8%
0 0.0%
0 0.0%
90.9% 9.1%
0 0.0%
1 0.9%
19 17.3%
0 0.9%
0 0.0%
95.0% 5.0%
0 0.0%
0 0.0%
1 0.9%
20 18.2%
1 0.9%
90.9% 9.1%
0 0.0%
0 0.0%
0 0.0%
2 1.8%
21 19.1%
91.3% 8.7%
100% 0.0%
90.9% 9.1%
86.4% 13.6%
90.9% 9.4%
95.4% 4.6%
92.8% 7.2%

(b)

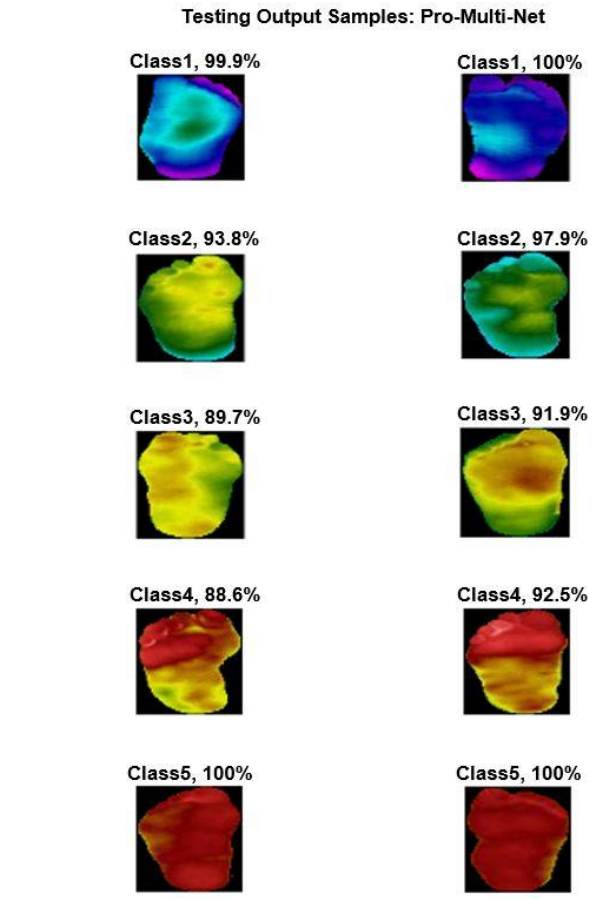

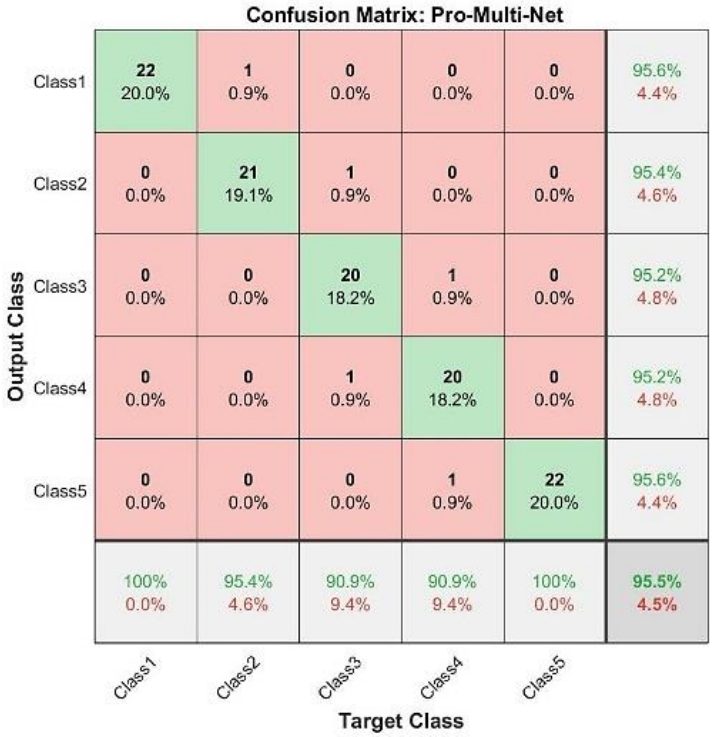

(c)

Fig 4.6 Testing Output Samples and Multiclassification Confusion Matrix for (a) DarkNet-19; (b) DarkNet-53 and (c) Pro-Multi-Net

DarkNet-19 gives better accuracy (89.2%), than the DL models implemented in previously reported work in multilevel foot thermogram classification [9]. But, it gives the minimal efficiency among the methods applied in this work. DarkNet-53 has higher overall percentage accuracy than DarkNet-19. Whereas, the proposed DL algorithm, Pro-Multi-Net is found to be the most efficient one. Table 4.6 records the performance metric values obtained and calculated by all the models for each class.

It can be deducted from Table 4.6 that for DarkNet-19 and DarkNet-53, class 1 (C_1) has the highest values for the three performance parameters, followed by class 5 (C_5). Also, C_3 gives the least precision for both these techniques. For DarkNet-19, C_4 has the minimal recall and F1-Score percentages. For DarkNet-53, recall values are minimal for C_2 and C_4. F1-Score is least for C_3.

Pro-Multi-Net achieves the greatest parameter values for two classes C_1 and C_5. Although, C_3 and C_4 give the lowest values among all levels (classes), there is increment in the percentage results for all the 5 classes in comparison to the rest two models.

Table 4.6 Performance Metric Calculations

DL NETWORK		**PERFORMANCE METRIC (%)**			
	C_n	***Precision***	***Recall***	***F1-Score***	***Accuracy***
DarkNet-19	**C_1**	95.4	95.4	95.4	89.2
	C_2	90.9	86.9	88.8	
	C_3	81.8	90.0	85.7	
	C_4	86.4	82.6	84.4	
	C_5	90.9	90.9	90.9	
DarkNet-53	**C_1**	100	95.6	97.7	92.8
	C_2	90.9	90.9	90.9	
	C_3	86.4	95.0	90.4	
	C_4	90.9	90.9	90.9	
	C_5	95.4	91.3	93.2	
Pro-Multi-Net	**C_1**	100	95.6	97.7	95.5
	C_2	95.4	95.4	95.4	
	C_3	90.9	95.2	93.0	
	C_4	90.9	95.2	93.0	
	C_5	100	95.6	97.7	

It can be inferred that the least performance measure percentages are obtained C_3 and C_4 because of the similar temperature patterns between them. Even though there are wider hot regions, there is no apparent difference. The results obtained are better in case of C_1, C_2 and C_5. This is because of the fact that C_1 consists of distributions without change in temperature. The transitions from C_1 to C_2 and from C_4 to C_5 are evident due to loss in butterfly pattern (C_2) and covering of the whole foot by hot region (C_5).

The conclusions drawn from this work and the future scope will be discussed in the following chapter.

CHAPTER - 5

CONCLUSION AND FUTURE SCOPE

This chapter explains the deductions obtained from the implementations of the deep learning methods including the proposed techniques in this work. Both binary and multi-level classification conclusions are discussed. Also, this chapter provides future visions of the work in this domain.

5.1 Conclusion

IR thermography has developed as an effective procedure in classifying and detecting DFUs. In this work, DL methods based on transfer learning have been implemented and analyzed comparatively in classification of foot thermograms. AlexNet has achieved greater accuracy than other methods reported in previous work. ResNet-101 is found to be more efficient than AlexNet as its network framework supports in solving waning gradient issue by the usage of identity mapping. AlexNet attains the minimal training time but also has the lowest performance.

In ProNet, training parameters are fine-tuned to achieve optimized performance. Also, dropout layers are inserted for dropping some inputs at random. This increases generalization as the layer learns using all its inputs. The proposed methodology has the best architectural features of ResNet and decremented layer count as in AlexNet. It is able to achieve the highest efficacy amongst all other techniques implemented. Thus, it can be effectively used in classifying DFUs with aid of thermograms.

For DFU classification, IR thermography has become a recognized technique in recent years. It is found to be advantageous for binary as well as multiclass classification DL networks. In this work, a comparative evaluation of three methods viz., DarkNet-19, DarkNet-53 and Pro-Multi-Net, the proposed network has been made for multiclass classification of DFU thermograms. The input thermographic images are classified into five levels on the basis of TCI values.

DarkNet-19 has attained greater accuracy and other performance metrics than the DL models applied in the existing work. As the network framework of DarkNet-53 contains residual layers, it is found to be more effective than DarkNet-19. These layers solve the degrading gradient problem. Although DarkNet-19 achieves the least training but also gives minimalistic performance.

Pro-Multi-Net, has optimum performance amongst all which combines the finest features of DarkNet-19 and DarkNet-53. For each class, it provides improved values of performance parameters. Also, dropout layers are added to enhance generalization because the layer learns to utilize all inputs to it. Precisely, the proposed algorithm is able to achieve a tradeoff between training time and the performance. Therefore, it can be efficiently used in classifying DFU thermograms into multiple classes.

5.2 Future Scope

Future scope exists in in upgrading of the DL algorithm structure for better learnability of image features. Also focus can be lied upon procurement of more number of foot thermograms. Furthermore, classification of DFUs can be investigated upon which comprise of relatively distinguishing color and texture features.

In future work, the network architecture can be enhanced so that feature learnability of images can be better. Moreover, foot ulcer thermograms which have distinctive color (also texture) features can be classified. There can be a focus on tuning the parameters more finely so as to differentiate the thermograms of third and fourth classes more efficiently. This will also increase the overall accuracy of the DL network. Furthermore, greater number of images can be collected. A less costly mini portable IR camera can be used to capture thermographic images.

REFERENCES

[1] Cho, N.H.; Kirigia, J.; Mbanya, J.C.; Ogurstova, K.; Guariguata, L.; Rathmann, W.; Roglic, G.; Forouhi, N.; Dajani, R.; Esteghamatil, A.; et al. IDF Diabetes Atlas, 8th ed.; IDF: Brussels, Belgium, 2017.

[2] Iversen, M.; Tell, G.; Riise, T.; Hanestad, B.; Østbye, T.; Graue, M.; Midthjell, K. History of foot ulcer increases mortality among individuals with diabetes: ten-year follow-up of the Nord-Trøndelag Health Study, Norway. Diabetes Care 2009, 32, 2193–2199

[3] W.H. Organization, Definition, diagnosis and classification of diabetes mellitus and its complications: report of a WHO consultation. Part 1, Diagnosis and classification of diabetes mellitus, 1999.

[4] Fauci, M. A., Breiter, R., Cabanski, W., Gunapala, S. D., Medical infrared imaging - Differentiating facts from fiction, and the impact of high precision quantum well infrared photodetector camera systems, and other factors, in its reemergence, Volume 42, Issues 3–5, June 2001, Pp. 337-344

[5] Bernard T.; D'Elia C.; Kabadi R; Wong N. An early detection system for foot ulceration in diabetic patients, Bioengineering Conference, 2009 IEEE 35th Annual Northeast, DOI: 10.1109/NEBC.2009.4967797

[6] J. Jiang, E.Y.K. Ng, A.C.B. Yeo, S. Wu, F. Pan, W.Y. Yau, J.H. Chen, Y. Yang, A perspective on medical infrared imaging, J. Med. Eng. Technol. 29 (6) (2005) 257–267.

[7] A. Szentkuti, H.A.N.A.S. Kavanagh, G. Simeon, Infrared thermography and image analysis for biomedical use, Period. Biol. 113 (4) (2011) 385–392.

[8] M. Diakides, J.D. Bronzino, D.R. Peterson (Eds.), Medical Infrared Imaging: Principles and Practices, CRC Press, Taylor & Francis Group, Boca Raton, FL, 2013.

[9] E.F.J. Ring, The historical development of temperature measurement in medicine, Infrared Phys. Technol. 49 (2007) 297–301.

[10] T. Nagase et al., Variations of plantar thermographic patterns in normal controls and non-ulcer diabetic patients: novel classification using angiosome concept, J. Plastic, Reconstruct. Aesthetic Surg. 64 (7) (2011) 860–866.

[11] B.B. Lahiri, S. Bagavathiappan, T. Jayakumar, J. Philip, Medical applications of infrared thermography: a review, Infrared Phys. Technol. 55 (2012) 221–235.

[12] C. Agurto et al., Characterization of diabetic peripheral neuropathy in infrared video sequences using independent component analysis, in: 2015 IEEE 25th International Workshop on Machine Learning for Signal Processing (MLSP). IEEE; 2015.

[13] G. Litjens, et al., A survey on deep learning in medical image analysis, Med. Image Anal. 42 (2017) 60–88.

[14] C. Szegedy, et al., in: Rethinking the inception architecture for computer vision, Proceedings of the IEEE Conference on Computer Vision and Pattern Recognition, 2016.

[15] Muhammad Adam, Eddie Y.K. Ng, Shu Lih Oh, Marabelle L. Heng, Yuki Hagiwara, Jen Hong Tan, Jasper W.K. Tong, U. Rajendra Acharya, Automated characterization of diabetic foot using nonlinear features extracted from thermograms, Infrared Physics & Technology, Volume 89, 2018, Pages 325-337.

[16] Cruz-Vega I, Hernandez-Contreras D, Peregrina-Barreto H, Rangel-Magdaleno JdJ, Ramirez-Cortes JM. Deep Learning Classification for Diabetic Foot Thermograms. Sensors. 2020; 20(6):1762.

[17] S. Bagavathiappan et al., Correlation between plantar foot temperature and diabetic neuropathy: a case study by using an infrared thermal imaging technique, J. Diabetes Sci. Technol. 4 (6) (2010) 1386–1392.

[18] M. Bharara et al., Applications of angiosome classification model for monitoring disease progression in the diabetic feet, Proceedings of the 2014 Summer Simulation Multiconference, Society for Computer Simulation International, 2014.

[19] D. Hernandez-Contreras, H. Peregrina-Barreto, J. Rangel-Magdaleno, J. Gonzalez-Bernal, Narrative review: diabetic foot and infrared thermography, Infrared Phys. Technol. 1350-449578 (2016) 105–117, https://doi. org/10.1016/j.infrared.2016.07.013.

[20] Mahnaz Etehadtavakol, E.Y.K. Ng, Naima Kaabouch, Automatic segmentation of thermal images of diabetic-at-risk feet using the snakes algorithm, Infrared Physics & Technology,Volume 86, 2017, Pages 66-76.

[21] Kaabouch, N., Hu, W.C., Yi Chen, Y.,"Alternative Technique to Asymmetry Analysis Based Overlapping for Foot Ulcer Examination: Scalable Scanning", J Diabetes Metab 2011, S:5Q

[22] Kaabouch, Naima, Yi Chen, Wen-Chen Hu, Julie Anderson, Forrest Ames, and Rolf Paulson. "Early detection of foot ulcers through asymmetry analysis." In SPIE Medical Imaging, International Society for Optics and Photonics, pp. 72621L-72621L, 2009

[23] Kaabouch, Naima, Yi Chen, Julie Anderson, Forrest Ames, and Rolf Paulson. "Asymmetry analysis based on Genetic Algorithms for the Prediction of Foot Ulcers." In IS&T/SPIE Electronic Imaging, International Society for Optics and Photonics, Pp: 724304-724304, 2009.

[24] Bernard T.; D'Elia C.; Kabadi R; Wong N. An early detection system for foot ulceration in diabetic patients, Bioengineering Conference, 2009 IEEE 35th Annual Northeast, DOI: 10.1109/NEBC.2009.4967797

[25] Bezdek, James C. (1981). Pattern Recognition with Fuzzy Objective Function Algorithms. ISBN 0-306- 40671-3, 1981.

[26] J.H. Tan, E.Y.K. Ng, U.R. Acharya, Evaluation of tear evaporation from ocular surface by functional infrared thermography, Med. Phys. 37 (11) (2010) 6022–6034.

[27] K.S. Vidya et al., Computer-aided diagnosis of myocardial infarction using ultrasound images with DWT, GLCM and HOS methods: a comparative study, Comput. Biol. Med. 62 (2015) 86–93

[28] S. Dua et al., Wavelet-based energy features for glaucomatous image classification, Ieee Trans. Inform. Technol. Biomed. 16 (1) (2012) 80–87.

[29] D. Giri et al., Automated diagnosis of coronary artery disease affected patients using LDA, PCA, ICA and discrete wavelet transform, Knowl.-Based Syst. 37 (2013) 274–282.

[30] R.M. Haralick, K. Shanmugam, Textural features for image classification, IEEE Trans. Syst., Man, Cybern. 6 (1973) 610–621.

[31] M.-K. Hu, Visual pattern recognition by moment invariants, IRE Trans. Inform. Theory 8 (2) (1962) 179–187.

[32] T. Ojala, M. Pietikainen, T. Maenpaa, Multiresolution gray-scale and rotation invariant texture classification with local binary patterns, IEEE Trans. Pattern Anal. Mach. Intell. 24 (7) (2002) 971–987.

[33] V.P. Singh, Entropy Theory and Its Application in Environmental and Water Engineering, John Wiley & Sons, 2013.

[34] Q. Hu, D. Yu, Entropies of fuzzy indiscernibility relation and its operations, Int. J. Uncertainty, Fuzziness Knowledge-based Syst. 12 (05) (2004) 575–589.

[35] Sudha Bandalakunta Gururajarao, Umadevi Venkatappa, Joshi Manisha Shivaram, Mohamed Yacin Sikkandar, Abdullah Al Amoudi, Chapter 4 - Infrared Thermography and Soft Computing for Diabetic Foot Assessment, Editor(s): Nilanjan Dey, Surekha Borra, Amira S. Ashour, Fuqian Shi, Machine Learning in Bio-Signal Analysis and Diagnostic Imaging, Academic Press, 2019, Pages 73-97.

[36] B.G. Sudha, V. Umadevi, J.M. Shivaram, Thermal image acquisition and segmentation of human foot, in: 4th International Conference on Signal Processing and Integrated Networks (SPIN), Noida, 2017, pp. 80–85, https://doi.org/10.1109/SPIN.2017.8049920.

[37] D. Hernandez-Contreras, H. Peregrina-Barreto, J. Rangel-Magdaleno, J.A. Gonzalez-Bernal, L. Altamirano-Robles, A quantitative index for classification of plantar thermal changes in the diabetic foot, Infrared Phys. Technol. 81 (2017) 242–249.

[38] J. Saminathan, M. Sasikala, VB. Narayanamurthy, K. Rajesh, R. Arvind, Computer aided detection of diabetic foot ulcer using asymmetry analysis of texture and temperature features, Infrared Physics & Technology,Volume 105, 2020, 103219.

[39] Patrick Nigri Happ, Raul Queiroz Feitosa, Cristiana Bentes, Ricardo Farias, A region-growing segmentation algorithm for GPUs, IEEE Geosci. Remote Sens. Lett. 10 (6) (2013) 1612–1616.

[40] A.J.M. Boulton, F.A. Gries, J.A. Jervell, Guidelines for the diagnosis and outpatient management of diabetic peripheral neuropathy, Diabet. Med. 15 (6) (1998) 508–514.

[41] Audrey Macdonald, Nina Petrova, Suhail Ainarkar, John Allen, Peter Plassmann, Aaron Whittam, John Bevans, Francis Ring, Ben Kluwe, Rob Simpson, Leon Rogers, Graham Machin, Mike Edmonds, Thermal symmetry of healthy feet: a precursor to a thermal study of diabetic feet prior to skin breakdown, Physiol. Measur. Inst. Phys. Eng. Med. 38 (2017) 33–44

[42] Robert M. Haralick, K. Shanmugam, Its'hak Dinstein, Textural features for image classification, IEEE Trans. Syst. Man Cybernet. 3 (6) (1973) 610–621.

[43] Leen-Kiat Soh, Costas Tsatsoulis, Texture analysis of SAR sea ice imagery using gray level co-occurrence matrices, IEEE Trans. Geosci. Remote Sens. 37 (2) (1999) 780–795.

[44] M. Sasikala, N. Kumaravel, A wavelet-based optimal texture feature set for classification of brain tumours, J. Med. Eng. Technol. 32 (3) (2008) 198–205.

[45] Hernandez-Contreras, D.A.; Peregrina-Barreto, H.; de Jesus Rangel-Magdaleno, J.; Renero-Carrillo, F.J. Plantar Thermogram Database for the Study of Diabetic Foot Complications. IEEE Access 2019, 7, 161296–161307.

[46] S. Albawi, T. A. Mohammed and S. Al-Zawi, "Understanding of a convolutional neural network," 2017 International Conference on Engineering and Technology (ICET), 2017, pp. 1-6, doi: 10.1109/ICEngTechnol.2017.8308186.

[47] Alzubaidi, L., Zhang, J., Humaidi, A.J. *et al.* Review of deep learning: concepts, CNN architectures, challenges, applications, future directions. *J Big Data* **8,** 53 (2021). https://doi.org/10.1186/s40537-021-00444-8

[48] Zhuang, F., Qi, Z., Duan, K., Xi, D., Zhu, Y., Zhu, H., Xiong, H. and He, Q., 2020. A comprehensive survey on transfer learning. Proceedings of the IEEE, 109(1), pp.43-76.

[49] Hussain, M., Bird, J.J., Faria, D.R. (2019). A Study on CNN Transfer Learning for Image Classification. In: Lotfi, A., Bouchachia, H., Gegov, A., Langensiepen, C., McGinnity, M. (eds) Advances in Computational Intelligence Systems. UKCI 2018. Advances in Intelligent Systems and Computing, vol 840. Springer, Cham. https://doi.org/10.1007/978-3-319-97982-3_16

[50] Alom, M.Z., Taha, T.M., Yakopcic, C., Westberg, S., Sidike, P., Nasrin, M.S., Essen, B.C., Awwal, A.A., & Asari, V.K. (2018). The History Began from AlexNet: A Comprehensive Survey on Deep Learning Approaches. *ArXiv, abs/1803.01164*.

[51] H. Wu, M. Xin, W. Fang, H. Hu and Z. Hu, "Multi-Level Feature Network With Multi-Loss for Person Re-Identification," in IEEE Access, vol. 7, pp. 91052-91062, 2019, doi: 10.1109/ACCESS.2019.2927052.

[52] He, K., Zhang, X., Ren, S., Sun, J. (2016). Identity Mappings in Deep Residual Networks. In: Leibe, B., Matas, J., Sebe, N., Welling, M. (eds) Computer Vision – ECCV 2016. ECCV 2016. Lecture Notes in Computer Science(), vol 9908. Springer, Cham. https://doi.org/10.1007/978-3-319-46493-0_38

[53] Redmon, J., & Farhadi, A. (2017). YOLO9000: Better, Faster, Stronger. 2017 IEEE Conference on Computer Vision and Pattern Recognition (CVPR), 6517-6525.

[54] Bochkovskiy, A., Wang, C., & Liao, H.M. (2020). YOLOv4: Optimal Speed and Accuracy of Object Detection. ArXiv, abs/2004.10934.

[55] Redmon, Joseph and Ali Farhadi. “YOLOv3: An Incremental Improvement.” ArXiv abs/1804.02767 (2018): n. pag.

[56] Etter, D. M., Kuncicky, D. C., & Hull, D. W. (2002). Introduction to MATLAB. Hoboken, NJ, USA: Prentice Hall.

[57] Higham, Desmond J., and Nicholas J. Higham. MATLAB guide. Society for Industrial and Applied Mathematics, 2016.

[58] Toolbox, Symbolic Math. "Matlab." Mathworks Inc (1993).

[59] Knight, A. (2019). Basics of MatLab® and beyond. Chapman and Hall/CRC.

[60] Ruder, S. (2016). An overview of gradient descent optimization algorithms. ArXiv, abs/1609.04747.

[61] Canbek, G., Sagiroglu, S., Temizel, T. T., & Baykal, N. (2017, October). Binary classification performance measures/metrics: A comprehensive visualized roadmap to gain new insights. In 2017 International Conference on Computer Science and Engineering (UBMK) (pp. 821-826). IEEE.

[62] Teng, Y., Gao, W., Chalus, F., Choromańska, A., Goldfarb, D., & Weller, A. (2019). Leader Stochastic Gradient Descent for Distributed Training of Deep Learning Models. NeurIPS.

[63] Manliguez, Cinmayii. (2016). Generalized Confusion Matrix for Multiple Classes. 10.13140/RG.2.2.31150.51523.

[64] Grandini, M., Bagli, E., & Visani, G. (2020). Metrics for multi-class classification: an overview. arXiv preprint arXiv:2008.05756.

[65] Sokolova, M., & Lapalme, G. (2009). A systematic analysis of performance measures for classification tasks. Information Processing and Management, 45, p. 427-437.

LIST OF PUBLICATIONS

Accepted Research Papers

1. **Title:** An Enhanced Methodology for Diabetic Foot Thermogram Classification using Deep Learning
   Authors: Aarushi Jain, Indu Sreedevi
   Conference: IEEE International Conference on "Machine Learning, Big Data, Cloud and Parallel Computing: Trends, Perspectives and Prospects" (Com-IT-Con-2022)
   Date of paper acceptance: 26th March 2022
   Conference Dates: 26th - 27th May 2022

2. **Title:** An Improved Deep Neural Network for Multiclass Classification of Diabetic Foot Thermogram
   Authors: Aarushi Jain, Indu Sreedevi
   Conference: CONIT 2022: International Conference on Intelligent Technologies (IEEE 2nd CONIT)
   Date of paper acceptance: 23rd April 2022
   Conference Dates: 24th to 26th June 2022

PAPER NAME

Thesis_M.tech_Aarushi.pdf

AUTHOR

Aarushi

WORD COUNT

8526 Words

CHARACTER COUNT

44133 Characters

PAGE COUNT

54 Pages

FILE SIZE

3.2MB

SUBMISSION DATE

May 17, 2022 11:08 AM GMT+5:30

REPORT DATE

May 17, 2022 11:08 AM GMT+5:30

2% Overall Similarity

The combined total of all matches, including overlapping sources, for each database.

- 1% Internet database
- 1% Publications database
- Crossref database
- Crossref Posted Content database

Excluded from Similarity Report

- Submitted Works database
- Bibliographic material

2% Overall Similarity

Top sources found in the following databases:

- 1% Internet database
- 1% Publications database
- Crossref database
- Crossref Posted Content database

TOP SOURCES

The sources with the highest number of matches within the submission. Overlapping sources will not be displayed.

1	bmcmedinformdecismak.biomedcentral.com Internet	<1%
2	d-nb.info Internet	<1%
3	D. Hernandez-Contreras, H. Peregrina-Barreto, J. Rangel-Magdaleno, J... Crossref	<1%
4	Muhammad Adam, Eddie Y.K. Ng, Shu Lih Oh, Marabelle L. Heng, Yuki ... Crossref	<1%
5	"Biometric Recognition", Springer Science and Business Media LLC, ... Crossref	<1%
6	Aleka Melese Ayalew, Ayodeji Olalekan Salau, Bekalu Tadele Abeje, Bel... Crossref	<1%
7	repositorio-aberto.up.pt Internet	<1%
8	spiedigitallibrary.org Internet	<1%
9	theses.ubn.ru.nl Internet	<1%

10	Amith Khandakar, Muhammad Chowdhury, Mamun Reaz, Sawal Ali et a... Crossref	<1%
11	jerryan.medium.com Internet	<1%
12	link.springer.com Internet	<1%
13	Predictive Analytics with Microsoft Azure Machine Learning, 2015. Crossref	<1%